JBC RESEARCH ARTICLE

The RNA-binding protein ZC3H11A interacts with the nuclear poly(A)-binding protein PABPN1 and alters polyadenylation of viral transcripts

Received for publication, March 9, 2023, and in revised form, June 9, 2023 Published, Papers in Press, June 23, 2023,
https://doi.org/10.1016/j.jbc.2023.104959

Katharina Kases[1,‡], Erik Schubert[1,‡], Zamaneh Hajikhezri[1], Mårten Larsson[1], Priya Devi[1], Mahmoud Darweesh[1,2], Leif Andersson[1], Göran Akusjärvi[1], Tanel Punga[1,*,‡], and Shady Younis[1,3,*,‡]

From the [1]Department of Medical Biochemistry and Microbiology, Uppsala University, Uppsala, Sweden; [2]Department of Microbiology and Immunology, Al-Azhr University, Assiut, Egypt; [3]Division of Immunology and Rheumatology, Stanford University, Stanford, California, USA

Reviewed by members of the JBC Editorial Board. Edited by Craig Cameron

Nuclear mRNA metabolism is regulated by multiple proteins, which either directly bind to RNA or form multiprotein complexes. The RNA-binding protein ZC3H11A is involved in nuclear mRNA export, NF-κB signaling, and is essential during mouse embryo development. Furthermore, previous studies have shown that ZC3H11A is important for nuclear-replicating viruses. However, detailed biochemical characterization of the ZC3H11A protein has been lacking. In this study, we established the ZC3H11A protein interactome in human and mouse cells. We demonstrate that the nuclear poly(A)-binding protein PABPN1 interacts specifically with the ZC3H11A protein and controls ZC3H11A localization into nuclear speckles. We report that ZC3H11A specifically interacts with the human adenovirus type 5 (HAdV-5) capsid mRNA in a PABPN1-dependent manner. Notably, ZC3H11A uses the same zinc finger motifs to interact with PABPN1 and viral mRNA. Further, we demonstrate that the lack of ZC3H11A alters the polyadenylation of HAdV-5 capsid mRNA. Taken together, our results suggest that the ZC3H11A protein may act as a novel regulator of polyadenylation of nuclear mRNA.

RNA-binding proteins (RBPs) control multiple steps in gene expression, including gene transcription, RNA export, RNA stability, and mRNA translation (1, 2). The RBPs directly interact with the target mRNAs and make multiple contacts with other proteins to achieve temporal and spatial regulation of gene expression. ZC3H11A is an RNA-binding protein with three uncharacterized CCCH-type zinc finger motifs (ZFM) present at the N-terminus of the protein (3). Several studies have shown that ZC3H11A is a subunit of the Transcription-Export (TREX) complex responsible for the nuclear mRNA export (4–8). TREX is a multiprotein complex containing the hexameric core THO complex (THOC1, THOC2, THOC3, THOC5, THOC6, and THOC7), which in turn associates with several subunits including ZC3H11A (9). Essential for TREX-mediated mRNA export is its interaction with properly processed mRNAs (10, 11). Therefore, different TREX complex subunits associate with the mRNA 5′ cap structure (NCBP1, NCBP3), exon junctions (DDX39A/B, ALYREF(THOC4), UIF, LUZP4, CHTOP), and the 3′ end poly(A) tail (THOC5, ZC3H14) (9, 11–14). Further, the TREX complex stimulates the m6A reader protein YTHDC1 recruitment to mRNA and favors exporting m^{6}A-modified mRNA (15). Together, these interactions ensure that capped, spliced, polyadenylated, and m^{6}A-modified mRNAs are recognized and efficiently exported from the nucleus. In addition to mRNA recognition, the TREX complex interacts with the nuclear pore complex (NPC) to accomplish mRNA export to the cytoplasm. The TREX subunit TAP/NXF1 mediates this interaction as it interacts with the nucleoporins at NPC and mRNA along with the ALYREF and THOC5 subunits (11, 16, 17).

Although the exact biochemical characteristics of ZC3H11A have remained enigmatic, it has been characterized as a heat shock-induced protein controlling virus growth (18–20). Four different human nuclear-replicating viruses (Human Immunodeficiency Virus 1 (HIV-1), Human Adenovirus 5 (HAdV-5), Influenza A virus, and Herpes Simplex Virus 1) showed reduced growth in HeLa cells lacking the ZC3H11A protein (19). Detailed studies have shown that the ZC3H11A protein was relocalized to replication centers in HAdV-5-infected HeLa cells and that a lack of ZC3H11A reduced cytoplasmic accumulation of some viral mRNAs, suggesting its role in virus mRNA processing and nuclear export (19). Similarly, a lack of the ZC3H11A protein affected porcine pseudorabies virus and porcine circovirus 2 amplification by reducing the cytoplasmic accumulation of viral mRNA in porcine cells (18). Collectively, the ZC3H11A protein is essential for virus replication, probably due to its role in TREX complex-mediated virus mRNA export (3, 18). Two very recent studies have further shed light on ZC3H11A functions. First, it has been shown that ZC3H11A is crucial for the viability and survival of mouse embryos (8). Notably, genetic characterization of *Zc3h11a*$^{-/-}$ mice embryos revealed dysregulation of the fatty acid and glycolysis pathways (8). Second, the human ZC3H11A protein can suppress NF-κB signaling, thereby controlling the

‡ These authors contributed equally to this work.
* For correspondence: Tanel Punga, tanel.punga@imbim.uu.se; Shady Younis, syounis@stanford.edu.

expression of several interferon-stimulated genes in HeLa cells (21).

The poly(A)-binding proteins (PABPs) are the proteins that specifically bind to polyadenosine (poly(A)) tails present at the 3′ end of mRNA. The PABPs are grouped based on their subcellular localization: (i) nuclear PABPs (PABPNs: PABPN1 and PABPN1L), and (ii) cytoplasmic PABPs (PABPCs: PABPC1, PABPC3, PABPC4, PABPC4L, PABPC5, and ePAB) (22). The PABPs lack catalytic domains but instead function as scaffold proteins as they bind to poly(A) tails *via* their RNA recognition motifs (23). The best-known function of PABPN1 is to stimulate poly(A) polymerase (PAP)-dependent polyadenylation (24, 25). In addition, PABPN1 can also define the poly(A) tail length as it mediates interactions between the PAP protein and the cleavage and specificity factor 1 (CPSF1) (25, 26). Historically, binding of the PABPN1 protein to poly(A) tails has been suggested to increase mRNA stability, nuclear mRNA export, and translation (27, 28). Surprisingly, PABPN1 also has an opposite role as it can promote the turnover of some of the host cell non-coding snoRNA host gene (SNHG) transcripts (29–31). Available data suggest that PABPN1 is a subunit of a poly(A) tail exosome targeting (PAXT) complex, which can target polyadenylated SNHG transcripts for degradation (30).

While ZC3H11A is essential for mouse development (8) and for the growth of multiple nuclear-replicating viruses (18, 19), the detailed biochemical characterization of the protein has been lacking. Therefore, the present study aimed to reveal the biochemical characteristics of the human ZC3H11A protein and correlate them to its functions.

Results

ZC3H11A interacts with the TREX complex in human and mouse cells

Our recent study established the ZC3H11A interactome in mouse embryonic stem cells (mESCs) (8). To understand whether the human ZC3H11A protein interactome differs from the mouse counterpart, we performed mass spectrometry (MS)-based proteomics analysis and compared the ZC3H11A protein interacting partners in human HeLa cells and mESCs as outlined in Figure 1*A*. Since nucleic acids can mediate protein–protein interactions, we treated the cell lysates with benzonase nuclease, which degrades both single- and double-stranded DNA and RNA. By doing that, we expected to identify direct protein-protein interactions not bridged by nucleic acids. The results of HeLa and mESCs MS analyses showed a significant interaction between ZC3H11A and proteins involved in mRNA processing (capping and splicing), mRNA export, and mRNA 3′ end processing (Figs. 1*B* and S1). The most significant ZC3H11A-interacting partners both in the mESCs and in HeLa cells were the TREX complex subunits (the THOC proteins, EIF4A3, ALYREF, CHTOP, POLDIP3) and PABPN1 (Fig. 1*C*). While it is known that ZC3H11A copurifies with the TREX complex subunits, its interaction with the PABPN1 protein has not been characterized previously.

The ZC3H11A zinc finger motifs mediate interactions with the PABPN1 protein

Our previous study showed that deletion of the three ZC3H11A zinc finger motifs (ZFMs, deletion referred to as dZF) affected ZC3H11A functions (19). To further reveal the details of the human ZC3H11A interactome, we overexpressed the GFP-ZC3H11A(wt) and GFP-ZC3H11A(dZF) proteins in parallel and affinity purified the proteins to identify interacting partners by MS, as depicted in Figure 2*A*. In line with its proposed mRNA export function (6, 8–10, 17), the GFP-ZC3H11A(wt) protein specifically interacted with several of the known TREX complex subunits (THOC1, THOC2, THOC6, DDX39B, CHTOP, POLDIP3, RBM8A, and ALYREF) and again with the PABPN1 protein (Fig. 2*B*). Notably, the interaction between ZC3H11A and PABPN1 was significantly reduced by the deletion of the ZFMs (Fig. 2*C*). On the other hand, interactions between ZC3H11A and some of the TREX complex proteins THOC2, POLDIP3, and ALYREF were not affected by the same deletion (Fig. 2*D*). To confirm that our results were not biased due to the N-terminal GFP-tag, we overexpressed and immunopurified the ZC3H11A(wt)-Flag protein in HeLa cells and analyzed the interacting proteins by MS. Similar to the GFP-ZC3H11A(wt), the ZC3H11A(wt)-Flag protein interacted with the PABPN1 protein (Fig. S2). Our MS-based findings encouraged us to investigate how the individual ZFMs contribute to the ZC3H11A protein function and its interaction with the PABPN1 protein.

Individual zinc finger motifs control ZC3H11A binding to PABPN1

To better understand the human ZC3H11A protein functions, we focused on its interaction with the PABPN1 protein as both proteins localize into nuclear speckles (Fig. S3) and impact the mRNA nuclear export (19, 32, 33). The ZC3H11A protein contains three CCCH-type ZFMs at the N-terminus of the protein (Fig. 3*A*). Since the functions of single ZFMs have not been studied, we mutated individual ZFMs by replacing the first cysteine in the CCCH motif with an alanine (CCCH > ACCH). This type of mutation reduces Zn^{2+}-binding by disrupting the formation of a functional ZFM (34). First, we tested whether the triple cysteine mutation (C8A/C37A/C66A, referred to as 3C>A) alters ZC3H11A binding to PABPN1. Indeed, the 3C>A mutation blocked ZC3H11A interaction with PABPN1 (Fig. 3*B*). Also, a deletion mutant ZC3H11A(dZF) was deficient in binding to PABPN1. To further delineate the role of ZFMs, we tested how individual ZFM mutations affect ZC3H11A binding to PABPN1. Notably, mutations within the first (C8A) and third (C66A) ZFM eliminated binding, whereas the C37A mutation reduced ZC3H11A binding to PABPN1 (Fig. 3*C*). ZC3H11A and PABPN1 are RNA-binding proteins; hence, RNA might mediate their mutual interaction. Therefore, we tested the ZC3H11A-PABPN1 interaction in the RNaseA/T1-, benzonase-, or RNase I-treated cell lysates. Neither RNaseA/T1 nor benzonase treatments did affect ZC3H11A-PABPN1 interaction, whereas, in RNase I-treated lysates, the interaction was

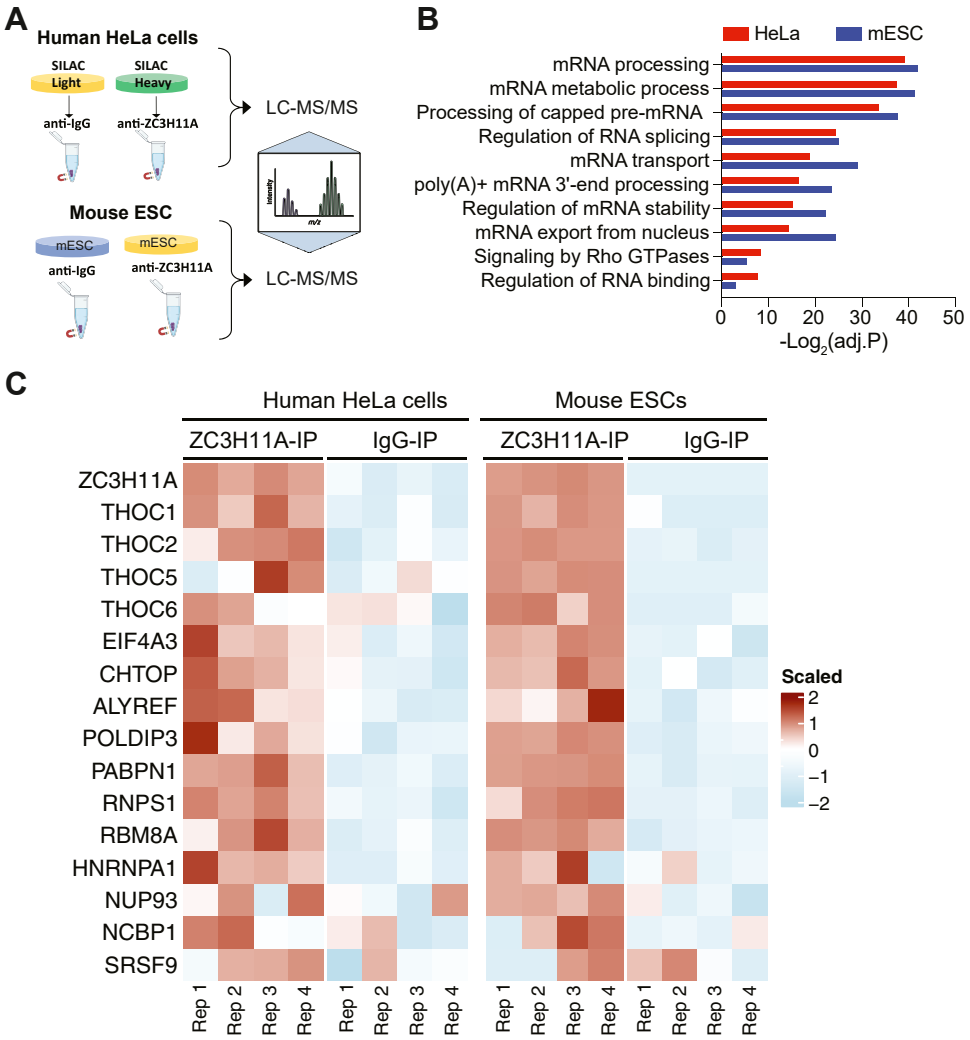

Figure 1. A comparison between the human and mouse ZC3H11A interactome. *A*, schematic illustration of the co-immunoprecipitation (co-IP) mass spectrometry (MS)-based experiments using the anti-ZC3H11A and anti-IgG antibodies in human HeLa cells and mouse embryonic stem cells (mESCs). *B*, pathway analysis of the identified interacting partners with endogenous ZC3H11A in HeLa cells and mESCs. *C*, heatmap of endogenous ZC3H11A-interacting partners involved in RNA export and 3′ end processing, based on ZC3H11A co-IPs in HeLa cells and mESCs. The heatmap represents the scaled values of log2-intensity of the indicated proteins (adjusted $p < 0.05$).

slightly reduced (Fig. 3*D*). Notably, RNase I degrades single-stranded RNA to nucleoside 3′-monophosphates, whereas RNaseA/T1 specifically degrades single-stranded RNA at C, U, and G nucleotides but not at A nucleotides. Hence, the ZC3H11A-PABPN1 interaction may be partially mediated/enhanced by single-stranded, A nucleotide-containing RNA sequences, like the poly(A) tail. Since ZC3H11A interacts with the THOC proteins (Fig. 1*C*) (6, 9), we tested if the ZFM mutations also affected ZC3H11A binding to two THOC proteins: THOC1 and THOC5. Both tested proteins interacted with both the wild-type and 3C>A mutant proteins (Fig. 3, *E* and *F*), confirming our MS-based analysis (Fig. 2*D*) that some of the THO complex members interact with ZC3H11A independently of the ZFMs.

Collectively, our data indicate that human ZC3H11A specifically associates with PABPN1 *via* ZFMs and that the first and third ZFM preferentially mediates this binding.

Zinc finger motifs are needed for ZC3H11A localization into nuclear speckles

ZC3H11A and PABPN1 are nuclear proteins with characteristic localization in the nuclear speckles (Fig. S3) (33). Nuclear speckles (NS) are distinct nuclear structures containing the proteins involved in mRNA processing and export (33). Therefore, we analyzed whether individual ZFM mutations alter ZC3H11A localization into NS. To this end, we performed indirect immunofluorescence experiments in HeLa cells transiently expressing the ZC3H11A-Flag proteins, followed by detecting both endogenous PABPN1 and transfected ZC3H11A-Flag proteins. Similar to the previous study (19), the ZC3H11A protein was detected in distinct NS, which overlapped PABPN1 staining (Fig. 4). Analysis of different ZFM mutants revealed that the individual ZFMs mutations, C3>A, and dZF mutations expelled the ZC3H11A protein from the NS. Interestingly, all the tested mutant proteins showed strong

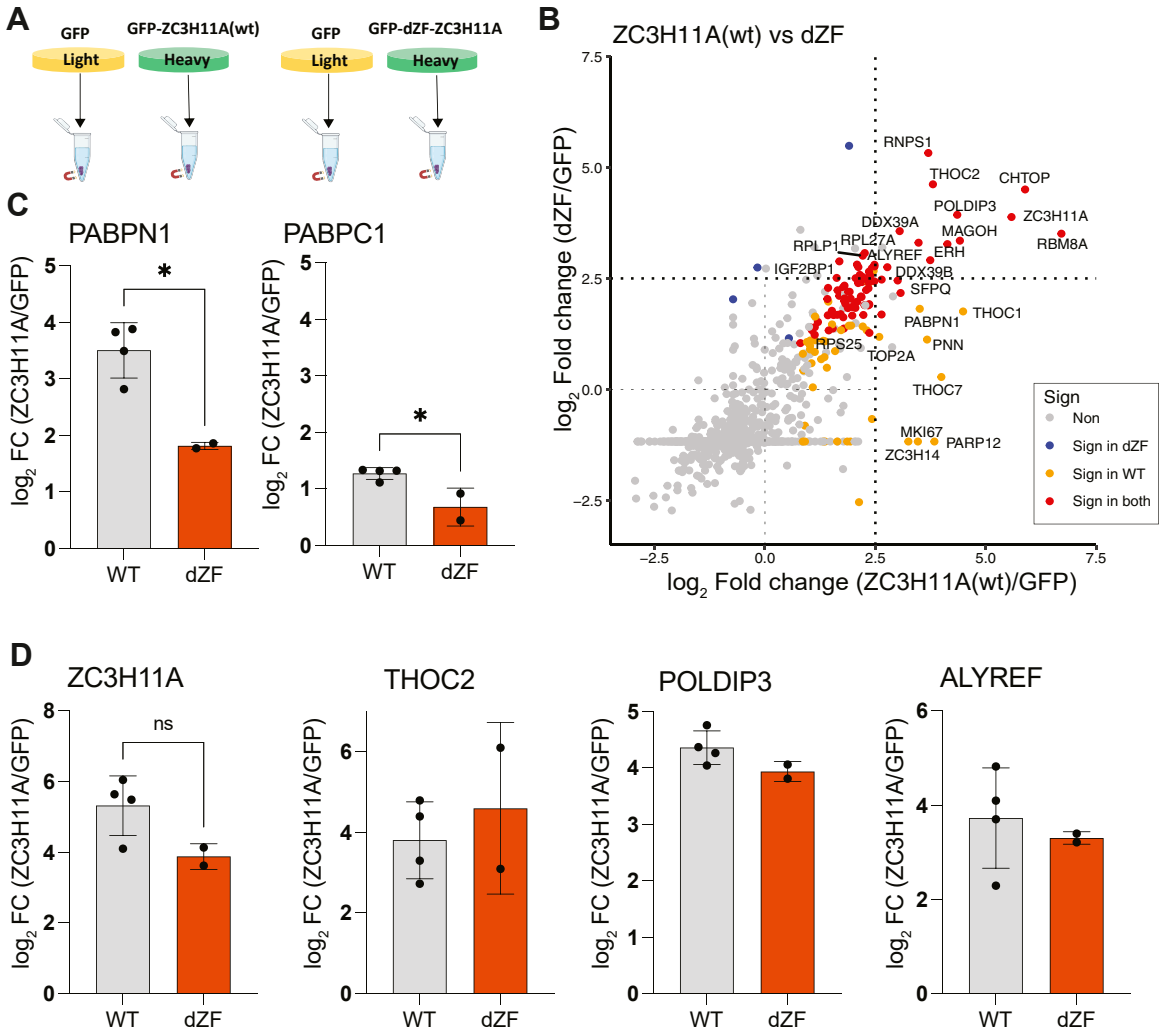

Figure 2. Human ZC3H11A protein interacts with the TREX complex subunits and PABPs. *A*, schematic illustration of the co-IP MS-based experiment using GFP, GFP-ZC3H11A(wt), and GFP-ZC3H11A(dZF) as the baits in HeLa cells. *B*, scatter plot showing enrichment of co-IP proteins from ZC3H11A(wt)/GFP *versus* ZC3H11A(dZF)/GFP proteins in HeLa cells. Sign: significant at adjusted $p < 0.05$ in the indicated condition. *C*, log2 enrichment of the PABPN1 and PABPC1 proteins interacting with the GFP-ZC3H11A(wt) or GFP-ZC3H11A(dZF) proteins. *D*, log2 enrichment of the ZC3H11A, THOC2, POLDIP3, and ALYREF proteins detected in the GFP-ZC3H11A(wt) *versus* GFP-ZC3H11A(dZF) co-IPs. Non, not significant.

nuclear staining, suggesting that ZFM mutations affect only localization to NS but not to the nucleus. Overall, our microscopy experiments support the co-immunoprecipitation experiments (Fig. 3), showing that the integrity of the individual ZFMs is needed to target ZC3H11A into the NS and mediate its binding to the PABPN1 protein.

PABPN1 retains ZC3H11A in the NS

Since our data indicate that ZC3H11A interacts with PABPN1 (Fig. 3) and that this interaction occurs in the NS (Figs. 4 and S3), we hypothesized that PABPN1 is needed for the ZC3H11A protein accumulation in the NS. To test this, we treated HeLa cells with siRNA against PABPN1 (siPABPN1) and analyzed the subcellular distribution of the ZC3H11A(wt)-Flag and ZC3H11A(dZF)-Flag proteins by indirect immunofluorescence. Notably, siPABPN1 treatment excluded the ZC3H11A(wt) protein from the NS into diffused nuclear staining (Fig. 5*A*). Remarkably, the diffused nuclear staining pattern of the ZC3H11A(wt)-Flag protein in siPABPN1-treated cells (Fig. 5*A*, the second-row images) resembled the PABPN1-binding deficient ZC3H11A(dZF)-Flag protein staining pattern in the siScr-treated cells (Fig. 5*A*, the third-row images). We also observed cytoplasmic, PABPN1 antibody-stained granules in siPABPN1-treated and ZC3H11A expressing cells (Fig. 5*A*). The origin, composition, and function of these granules remain unclear. To understand if the siPABPN1-treatment had a general effect on NS formation, the siPABPN1-treated cells were stained with an antibody detecting a known NS protein, the splicing factor SC35(SRSF2) (35). However, as shown in Figure 5*B*, the lack of PABPN1 did not detectably alter the SC35 protein localization.

Taken together, our data support the hypothesis that PABPN1 is needed for the localization of ZC3H11A into NS in HeLa cells.

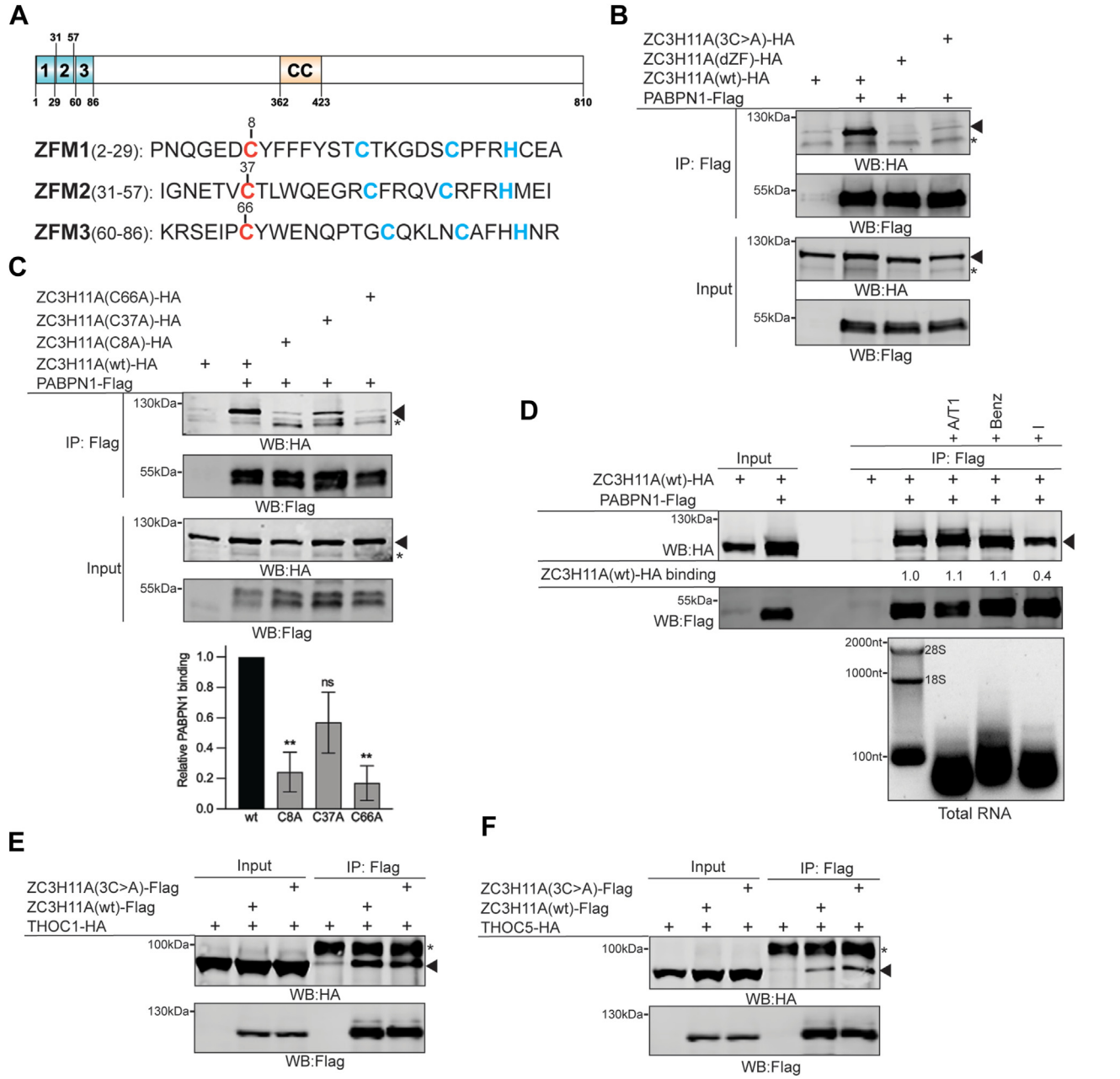

Figure 3. Zinc finger motifs control ZC3H11A binding to PABPN1. *A*, a schematic drawing of the human ZC3H11A protein. Individual zinc finger motifs (ZFM1-3) and coil-coiled domain (CC) are indicated based on the uniport.org (O75152) annotation. Individual CCCH motifs are shown (*red* and *blue*). Mutated cysteine (Cys(C) to Ala(A)) is indicated in *red*. *B*, co-IP of the HA-tagged ZC3H11A proteins using PABPN1-Flag as the bait in transfected HEK293T cells. The 3C>A mutant includes C8A, C37A, and C66A triple mutations, whereas the dZF mutant lacks the entire N-terminus of the protein. Western blot (WB) analysis with the anti-Flag and anti-HA antibodies. An *asterisk* indicates an unspecific protein; *arrowheads* indicate migration of the ZC3H11A protein. *C*, co-IP of the individual ZC3H11A ZFM mutants with the PABPN1-Flag protein as the bait. After normalization to input, the relative binding of the individual ZFM mutants to PABPN1 is shown below the image (ZC3H11A(wt) = 1). Data (mean ± SEM, $^{**}p \leq 0.01$) from three individual experiments. *D*, co-IP of ZC3H11A(wt)-HA with PABPN1-Flag as a bait in the RNase A/T1 (+A/T1), benzonase (+Benz) or RNase I (+I) treated cell lysates. Quantification of ZC3H11A(wt)-HA binding is shown below the anti-HA blot, ZC3H11A(wt)-HA interaction with PABPN1-Flag in non-treated cell lysates was considered 1. The efficiency of the nuclease treatments in the cell lysates is shown on an agarose gel image below the protein images. Migration of 28S and 18S rRNA and DNA molecular weight markers are indicated. *E*, co-IP of THOC1-HA with either ZC3H11A(wt)-Flag or ZC3H11A(3C>A)-Flag as the baits. *F*, co-IP of THOC5-HA with either ZC3H11A(wt)-Flag or ZC3H11A(3C>A)-Flag as the baits. An *asterisk* indicates an unspecific protein, whereas the arrowheads indicate migration of the THOC1-HA and THOC5-HA proteins.

The ZC3H11A protein contains two independent nuclear localization signals

Since the ZC3H11A protein showed intense nuclear staining, we wanted to know whether ZC3H11A contains a nuclear localization signal (NLS) driving its nuclear localization. The classical NLS (cNLS) is defined as a short, 4 to 8 amino acid sequence enriched with positively charged amino acids such as lysines (K) and arginines (R) (36). Bioinformatic analysis using the cNLS Mapper program revealed that the ZC3H11A protein contains a potential NLS between amino acids 284 to 304 (37). Since this region contains 3 K and 2 R residues, we generated a ZC3H11A mutant protein (KR5>A), where all five

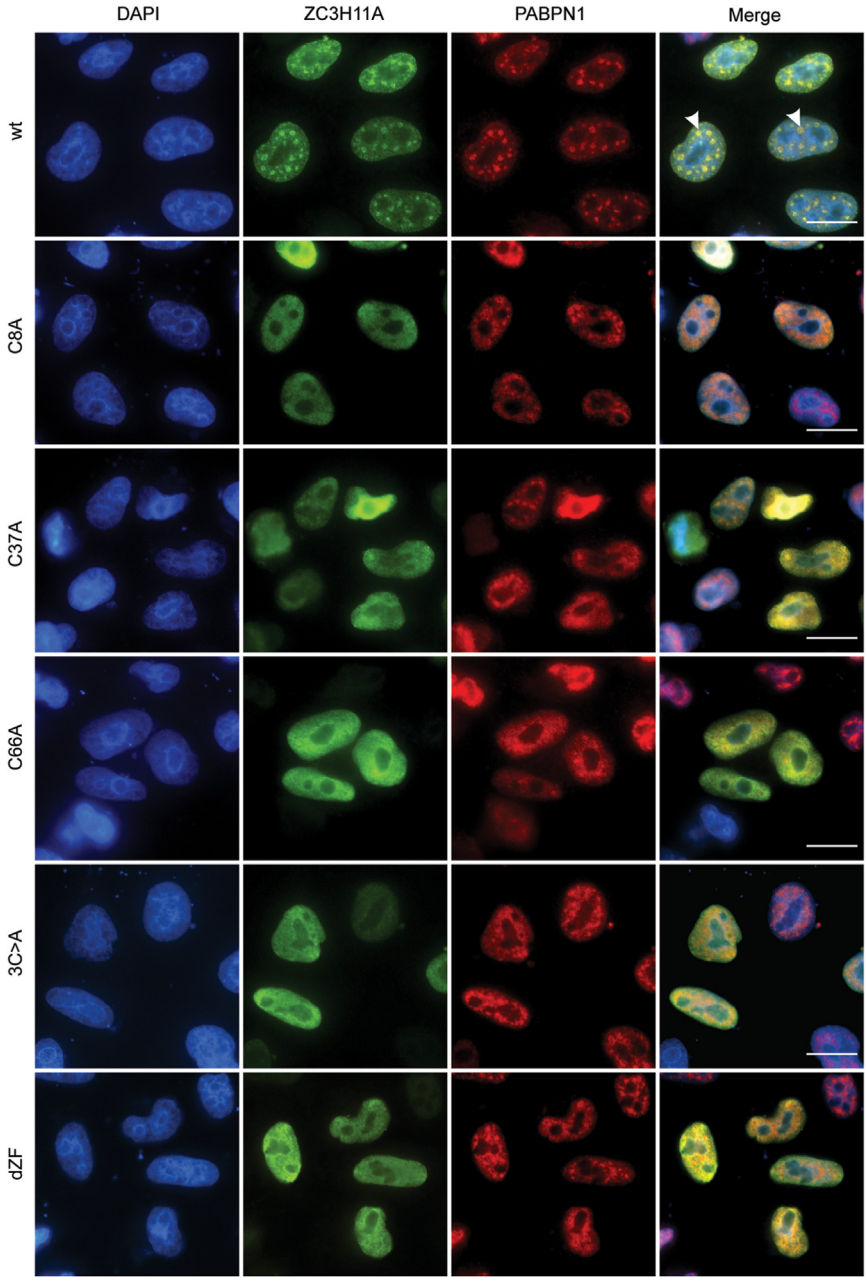

Figure 4. Zinc finger motifs are needed for ZC3H11A localization into nuclear speckles. HeLa cells were transfected with the respective ZC3H11A-Flag encoding plasmids for 24 h. Indirect immunofluorescence (IF) was done with the anti-Flag and anti-PABPN1 antibodies. Cells were counterstained with DAPI. Scalebar is 20 μm.

residues were exchanged for alanines (A). The KR5>A mutant protein was expressed and detected with immunofluorescence in HeLa cells. Surprisingly, the KR5>A mutant protein showed a very similar nuclear localization as did the ZC3H11A(wt)-Flag protein (Fig. 6*A*), suggesting that additional NLS may exist in the protein. This was also supported by the observation that the C-terminal deletion mutant ZC3H11A(1–280) showed apparent cytoplasmic staining, whereas mutant 1 to 530 was still found in the nucleus. Therefore, we generated two C-terminal deletion mutants using the ZC3H11A(KR5>A) sequence as the background. As shown in Figure 6*A*, deletion mutant KR5>A/1 to 660 showed intense cytoplasmatic staining, whereas the mutant KR5>A/1 to 749 was detected only in the nucleus. To further narrow potential NLS, we generated a deletion mutant protein lacking amino acids 661 to 699. The ZC3H11A(Δ661–699)-Flag protein still showed apparent NS staining, whereas the double mutant ZC3H11A(KR5>A/Δ661–699) was excluded from the nucleus. Hence, the ZC3H11A protein contains at least two independent NLSs: one between amino acids 284 to 304 and another between amino acids 661 to 699. This is also supported by our biochemical fractionation experiment where the ZC3H11A(wt)-Flag protein was detected only in the nucleus, whereas the double NLS mutant protein ZC3H11A(KR5>A/

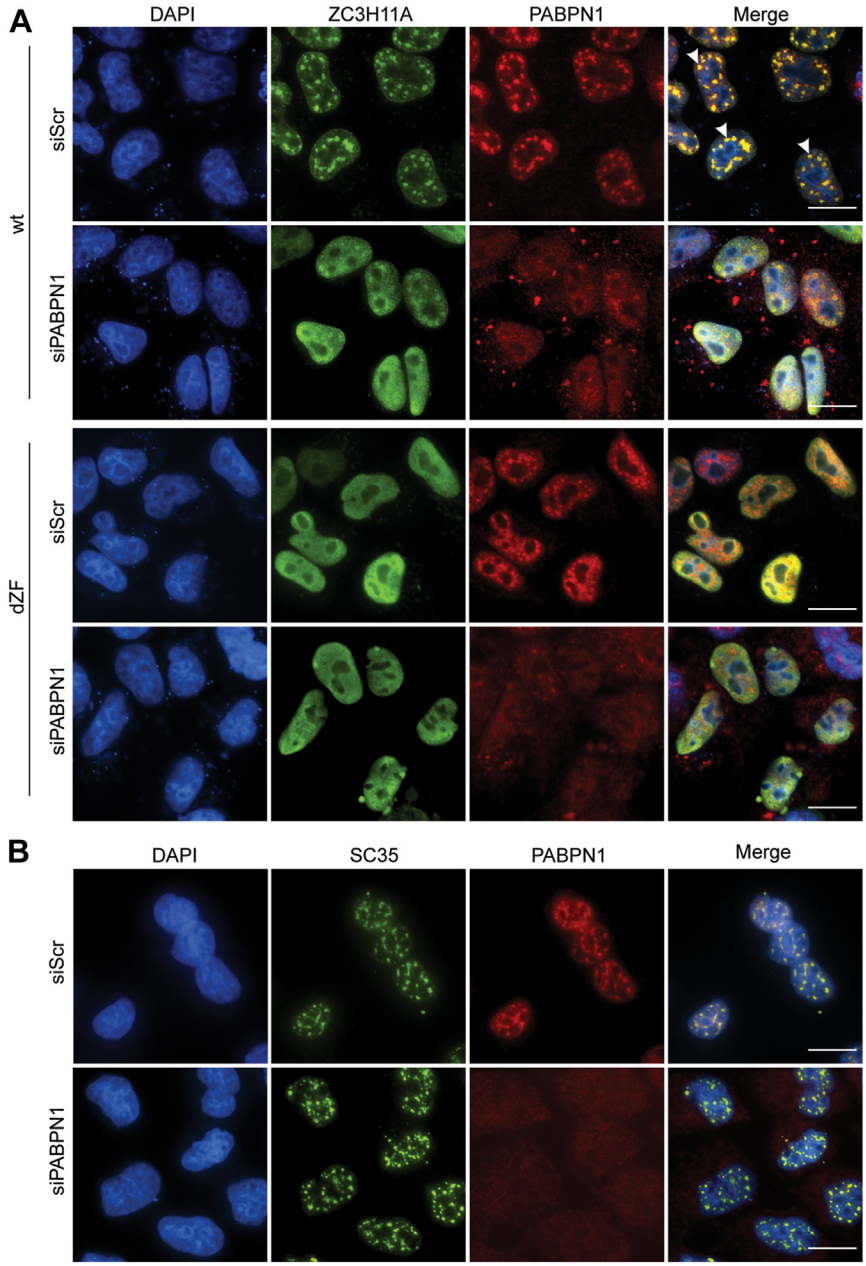

Figure 5. PABPN1 is needed for ZC3H11A localization into nuclear speckles. *A*, HeLa cells were treated with scrambled (siScR) or PABPN1-specific (siPABPN1) siRNAs (36 h) followed by transient expression of the ZC3H11A(wt)-Flag or ZC3H11A(dZF)-Flag proteins (24 h). IF was done using the anti-Flag and anti-PABPN1 antibodies. *B*, HeLa cells were treated with siScR or siPABPN1, followed by IF detection of the endogenous SC35 and PABPN1 proteins. Cells were counterstained with DAPI. Scalebar is 20 μm. Note that siPABPN1 efficiency in HeLa cells is shown in Figure 7*B*.

Δ661–699) was found in the cytoplasm and to some extent still in the nucleus (Fig. 6*B*).

If the ZC3H11A protein contains functional NLS, it should specifically interact with the importin receptors responsible for binding to NLS and nuclear delivery of the proteins (38). Therefore, we tested whether a known importin receptor, karyopherin subunit alpha 3 (KPNA3), which copurifies with the TREX complex (5), can bind to the ZC3H11A protein. The ZC3H11A(wt)-Flag specifically interacted with the endogenous KPNA3, whereas the NLS-deficient proteins either showed drastically reduced binding (Δ661–699) or lacked the binding (KR5>A/Δ661–699) (Fig. 6*C*). Our previous study showed that ZC3H11A is a relatively unstable protein (19). Therefore, we tested whether ZC3H11A subcellular localization influences its stability by treating ZC3H11A(wt)-Flag or ZC3H11A(KR5>A/Δ661–699)-Flag expressing HeLa cells with cycloheximide (CHX). The CHX treatment blocks *de novo* protein synthesis and therefore enables the detection of protein decay during a predefined time (39). Notably, the ZC3H11A(KR5>A/Δ661–699) protein was more resistant to degradation compared to the wild-type counterpart (Fig. 6*D*).

Overall, our results suggest that the ZC3H11A protein contains two independent NLS needed for nuclear localization and fast protein turnover.

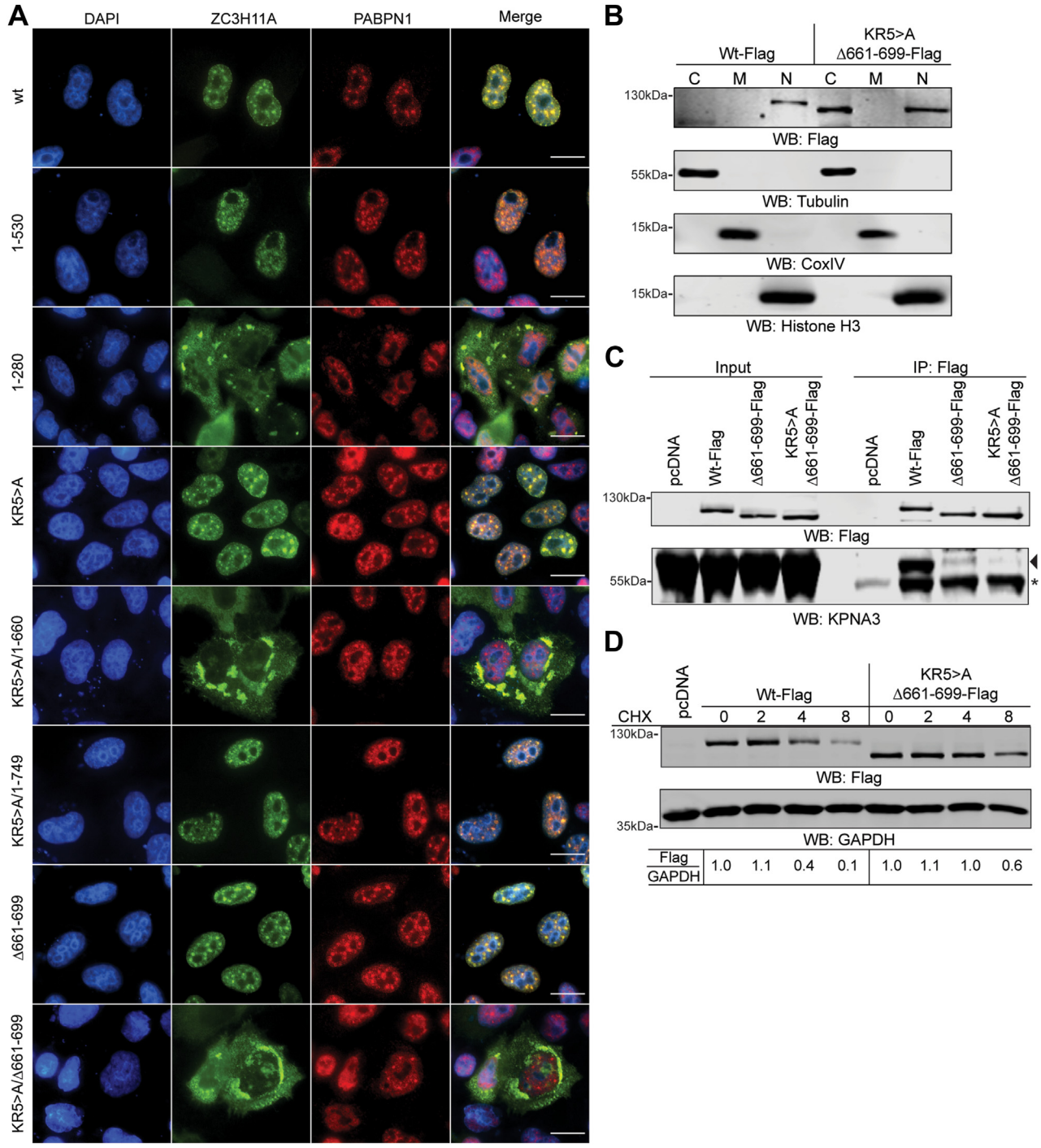

Figure 6. The ZC3H11A protein contains two independent nuclear localization signals. *A*, subcellular localization of the respective ZC3H11A-Flag proteins. IF was done using the anti-Flag and anti-PABPN1 antibodies, cells were counterstained with DAPI. Scalebar is 20 μm. *B*, biochemical fractionation of the ZC3H11A(wt)-Flag and NLS-deficient ZC3H11A(KR5>A/Δ661–699)-Flag proteins. WB analysis with the anti-Flag, anti-tubulin (a marker for cytoplasmic fraction), anti-CoxIV (a marker for mitochondrial fraction), and anti-histone H3 (a marker for nuclear fraction). *C*, co-IP of the endogenous KPNA3 using the ZC3H11A(wt)-Flag, ZC3H11A(Δ661–699)-Flag, and ZC3H11A(KR5>A/Δ661–699)-Flag proteins as the baits in HeLa cells. WB analysis with the anti-Flag and anti-KPNA3 antibodies. An *asterisk* marks an unspecific protein, whereas the arrowhead indicates the migration of the KPNA3 protein. *D*, cycloheximide (CHX) treatment of HeLa cells expressing the ZC3H11A(wt)-Flag or ZC3H11A(KR5>A/Δ661–699)-Flag proteins. Cells were collected at 0, 2, 4, and 8 h after adding CHX to the growth media. Relative ZC3H11A-Flag protein intensity is shown after normalization to the GAPDH protein. The protein signal at the time of adding CHX (t = 0) was considered as 1.

Lack of ZC3H11A alters mRNA polyadenylation

Our previous study showed that HAdV-5 lytic growth was reduced in ZC3H11A-lacking HeLa cells (19). Notably, the lack of ZC3H11A altered viral capsid mRNA export in this study. Since polyadenylation stimulates the mRNA export (40), we hypothesized that the ZC3H11A protein might interfere with HAdV-5 capsid mRNA polyadenylation. The HAdV-5 capsid precursor mRNA (pre-mRNA) is processed

into five different mRNA families (L1 to L5) due to the usage of different polyadenylation sites (L1 pA site to L5 pA site) (Fig. 7*A*) (41, 42). To test our hypothesis, we used the extension Poly(A) Test (ePAT), which is a PCR-based method where PCR amplicons reflect the actual length distribution of the poly(A) tail on the target mRNA (43). As the amplification control, a TVN-PAT reaction was used. Due to an anchored PCR primer, the TVN-PAT amplicon has an invariant poly(A)$_{12}$ tail, irrespective of the sample's actual poly(A) length (43). We used siRNAs to knock down protein expression to test the effect of ZC3H11A and PAPBPN1 on polyadenylation (Fig. 7*B*). As an additional control, cells were treated with an siRNA targeting the Cleavage and Polyadenylation Factor 1 (CPSF1), which is a subunit of the essential CPSF complex recognizing the poly(A) signal on the pre-mRNA (44). Analysis of the TVN-PAT amplicons revealed very similar PCR amplification at L3 and L5 pA sites in siScR- and siZC3H11A-treated samples (Fig. 7*C*). As expected, siCPSF1-treatment blocked PCR amplification, hence validating the specificity of the method. Also, the siPABPN1-treatment reduced the TVN-PAT signal, although not to the same extent as observed for siCPSF1. Interestingly, the ePAT reactions showed less intense (L3 and L5) and slower migrating (L3) amplicons in the siZC3H11A-treated samples (Fig. 7*C*). In line with the reduced TVN-PAT signal, the ePAT signal was almost undetectable in siPABPN1- and siCPSF1-treated cells. This indicates that lack of ZC3H11A alters the polyadenylation of viral transcripts using the L3 (*i.e.*, pVI, hexon) and L5 (*i.e.*, fiber) poly(A) sites (Fig. 7, *A* and *C*). In addition to its mRNA stabilizing role, the PABPN1 protein has been shown to cause SNHG RNA degradation as it is a subunit of the exonucleolytic PAXT complex (30). Therefore, we tested whether ZC3H11A alters the accumulation of PAXT-targeted SNHG10 and SNHG19 RNA (30). As shown in Figure 7*D*, siZC3H11A treatment did not change SNHG10 and SNHG19 RNA expression, whereas

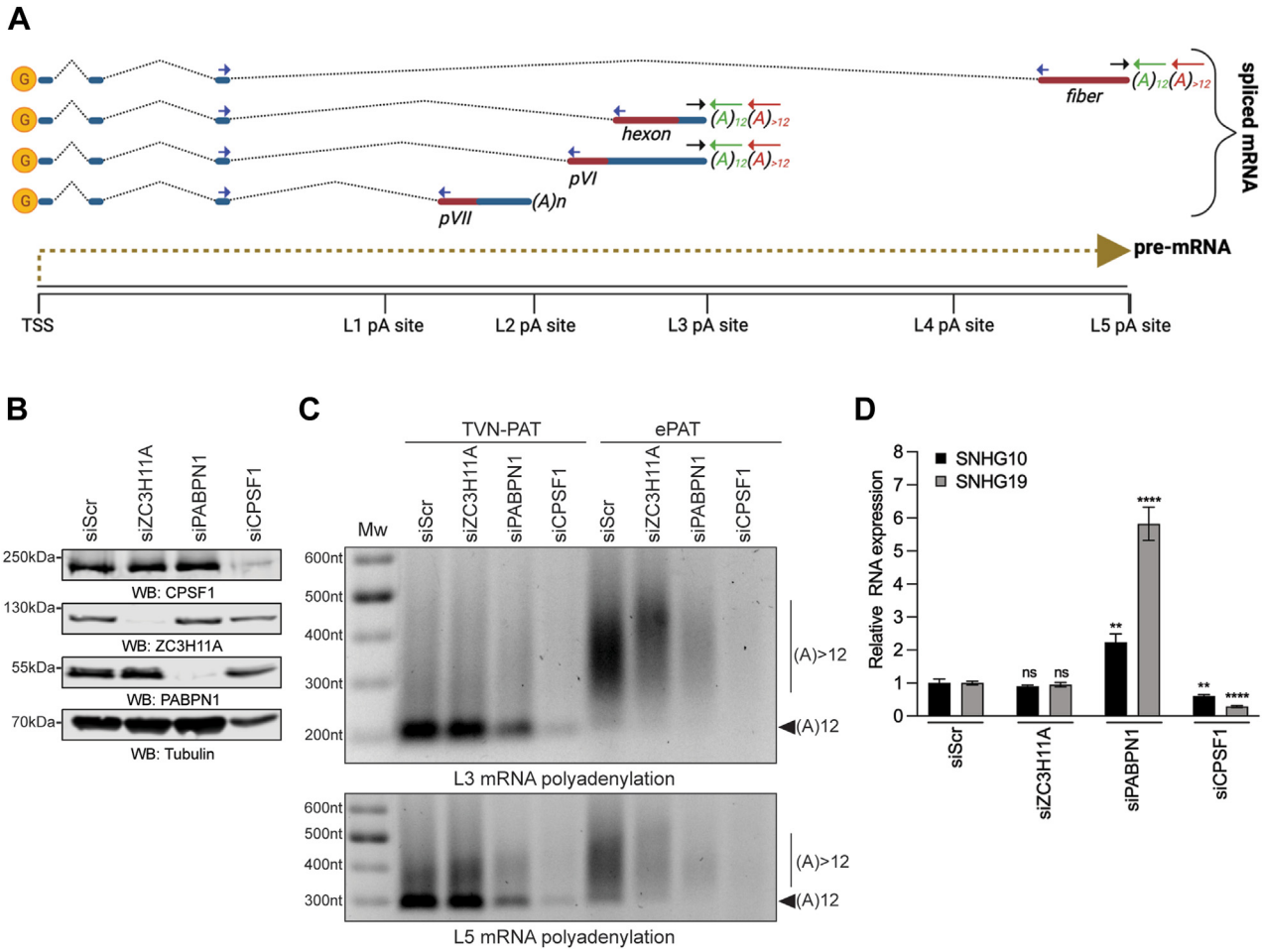

Figure 7. ZC3H11A deficiency alters HAdV-5 mRNA polyadenylation. *A*, simplified drawing of some HAdV-5 capsid mRNAs (pVII, pVI, hexon, fiber) originating from the virus major late transcription unit (MLTU). *Blue arrows* indicate spliced mRNA amplicons, *black* and *green arrows* indicate TVN-PAT amplicons, *while black* and *red arrows* indicate ePAT amplicons. *B*, WB from siRNA-treated HeLa cells. Proteins were detected with the anti-ZC3H11A, anti-PABPN1, anti-CPSF1, and anti-tubulin antibodies. *C*, total RNA from siRNA-treated and HAdV-5-infected samples was analyzed with ePAT and TVN-PAT methods. PCR amplicons detect HAdV-5 L3 and L5 poly(A) tails. An arrow with the label "(A)12" indicates the migration of mRNA with defined 12 As containing poly(A) tail. A vertical line with the label "(A) >12" indicates mRNA species with poly(A) tail longer than 12 As. *D*, expression of SNHG10 and SNHG19 RNA in siRNA-treated HeLa cells. HPRT1 was used to normalize SNHG expression. Data are shown as mean ± SD (****$p \le 0.0001$; **$p \le 0.01$; ns, not significant) from a triplicate experiment. The significance levels refer to comparisons with the siScr sample. G, capped nucleotide; pA, polyadenylation site; TSS, transcription start site.

siPABPN1-treatment elevated the levels of these two SNHG RNAs in HeLa cells.

Collectively, our data indicate that the ZC3H11A protein alters HAdV-5 capsid mRNA polyadenylation but is not engaged in cellular SNHG10 or SNHG19 RNA degradation.

ZC3H11A binds to HAdV-5 mRNA in a PABPN1-dependent manner

Since ZC3H11A ZFMs interact with polyadenylated mRNA (19) and the PABPN1 protein (Fig. 3), we hypothesized that PABPN1 might mediate ZC3H11A binding to mRNA. To test this, we analyzed ZC3H11A binding to some of the HAdV-5 capsid mRNAs (pVII, hexon, fiber) (Figs. 7*A* and 8*A*) in the lung epithelial cell line A549, a standard model cell line of many respiratory viruses, including HAdV-5 (45). First, we tested how different ZFM mutations influence ZC3H11A binding to viral mRNAs. As shown in Figure 8*A*, all ZFM mutants (C8A, C37A, C66A, C3>A) showed reduced binding to the tested viral transcripts. Interestingly, RNA-binding of the mutant C8A was mostly affected compared to other point mutant proteins. Notably, all the tested ZC3H11A proteins were expressed at a similar level in virus-infected A549 cells (Fig. S4). Since the same ZC3H11A mutant proteins were deficient in binding to PABPN1 (Fig. 3, *B* and *C*), we hypothesized that the PABPN1 protein might mediate ZC3H11A binding to viral mRNAs. In agreement with this hypothesis, siPABPN1-treatment blocked ZC3H11A binding to two of the tested viral transcripts (Fig. 8*B*). The ZC3H11A(wt)-Flag protein was immunopurified equally well from the siScr- and siPABPN1-treated cells, indicating that the reduced RNA-binding was not caused by a lower level of the ZC3H11A(wt)-Flag protein in the siPABPN1-treated cells (inserted panel in Fig. 8*B*). Proper processing of the capsid mRNAs is essential for forming infectious HAdV-5 particles. Therefore, we assumed that a lack of ZC3H11A should affect the production of infectious progeny virus in A549 cells. To test this, siZC3H11A- and siPABPN1-treated A549 cells were

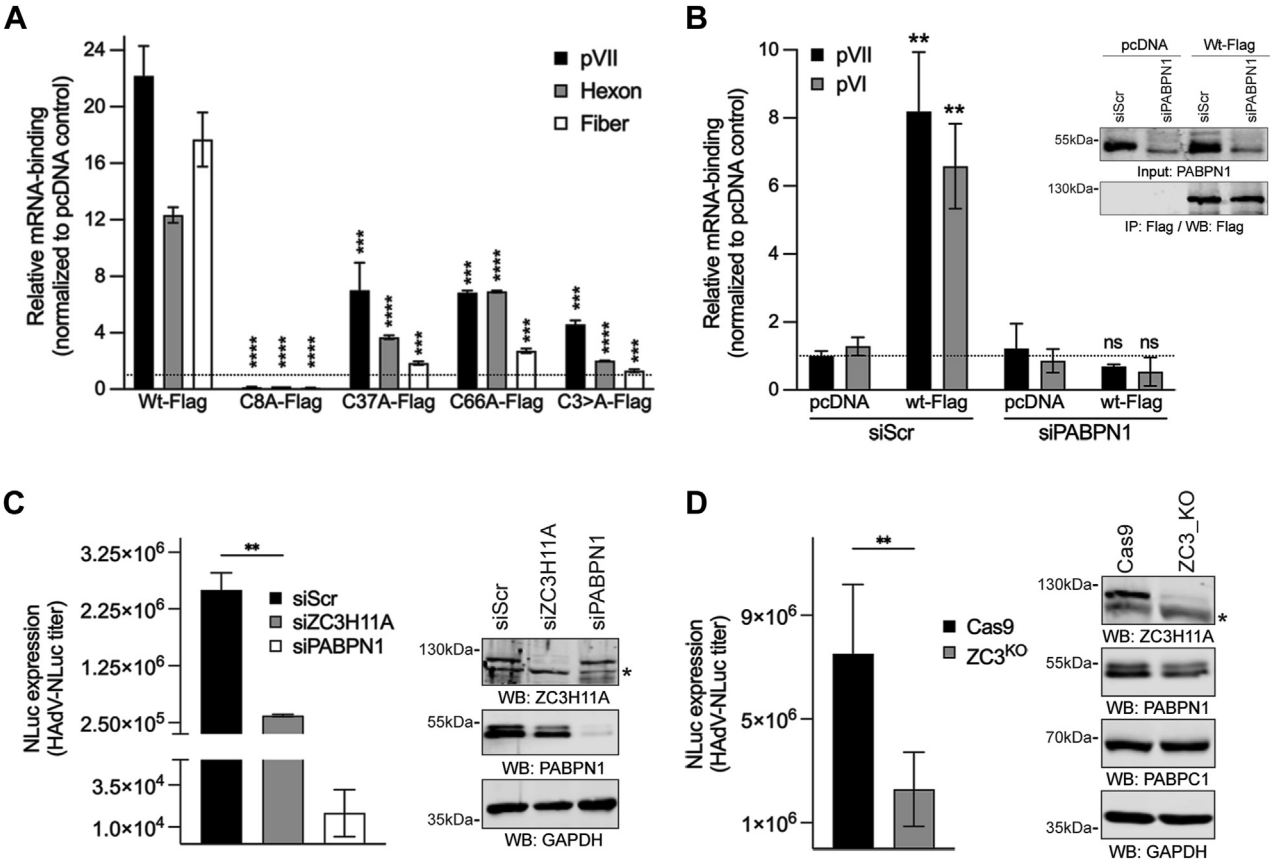

Figure 8. ZC3H11A binds to mRNA in a PABPN1-dependent manner. *A*, individual ZC3H11A-Flag proteins were immunoprecipitated from HAdV-5-infected (MOI = 5, 48 hpi) A549 cells and analyzed for binding to target mRNA (pVII, hexon, and fiber) using qRT-PCR. Data are shown relative mRNA enrichment in the ZC3H11A-Flag plasmid transfected samples compared to the control pcDNA plasmid transfected sample. Data (mean ± SD; ****$p \le 0.0001$; ***$p \le 0.001$) from a triplicate experiment. The significance levels refer to comparisons with the ZC3H11A(wt)-Flag sample. *B*, PABPN1 is needed for the ZC3H11A-Flag protein binding to mRNAs. The ZC3H11A(wt)-Flag protein was immunoprecipitated from siScr- or siPABPN1-treated (48 h) HAdV-5-infected A549 cells (MOI = 5, 24 hpi) and analyzed for viral mRNA (pVII and pVI) binding. Data (mean and ± SD; **$p \le 0.01$; ns, not significant) from a triplicate experiment. The significance levels refer to comparisons with the pcDNA sample. Western blot insert shows the equal recovery of the ZC3H11A(wt)-Flag protein from siScr- and siPABPN1-treated and HAdV-5-infected cells. *C*, formation of infectious progeny (HAdV-NLuc titer) in siRNA-treated A549 cells. Expression of the NanoLuc (NLuc) reporter gene was used as the read-out of infectious virus particles. NLuc values are shown as mean ± SD (**$p \le 0.01$) from a triplicate experiment. The significance levels refer to comparisons with the siScr sample. Western blot shows the efficiency of the siZC3H11A- and siPABPN1-treatment (48 h) in A549 cells. *D*, formation of infectious progeny in CRISPR/Cas9-modified A549 cells. Control (Cas9) and ZC3H11A modified (ZC3^{KO}) A549 cells were infected and analyzed as in *panel C*. Western blot showing lack of the ZC3H11A protein in CRISPR/Cas9 modified A549 cells. NLuc values are shown as mean ± SD (**$p \le 0.01$). The significance levels refer to comparisons with the Cas9 sample.

infected with a HAdV-5 virus expressing the NanoLuc (NLuc) reporter gene. Cell lysates were prepared 24 h post-infection (hpi) and used to re-infect HeLa cells, followed by NLuc measurement as an experimental read-out. If the lack of ZC3H11A affects virus mRNA polyadenylation, it should be reflected in the reduced formation of infectious virus particles in A549 cells. Re-infection of HeLa cells with the same volume of the cell lysate from siScr- or siZC3H11A-treated A549 cells should then show reduced reporter gene NLuc expression as less infectious virus particles are used to re-infect the HeLa cells. Indeed, both siZC3H11A- and PABPN1-treatments affected NLuc expression, with a more drastic effect in siPABPN1-treated cells (Fig. 8*C*). To further confirm these observations, we generated an A549 cell line ($ZC3^{KO}$) where the ZC3H11A protein expression was eliminated using the CRISPR/Cas9 editing approach. As shown in Figure 8*D*, NLuc reporter gene expression was reduced in HeLa cells re-infected with $ZC3^{KO}$ cell lysates.

Discussion

Most ZC3H11A functional studies reported so far are based on siRNA- or CRISPR/Cas9-based elimination of the ZC3H11A protein (18, 19, 21). In the present study, we reveal the human ZC3H11A protein interactome with a clear focus on characterizing the ZC3H11A-PABPN1 interaction. The most significant ZC3H11A-interacting proteins identified in this study were those involved in the mRNA processing, nuclear mRNA export, and mRNA 3′ end processing (Fig. 1, *B* and *C*). ZC3H11A interaction with the mRNA export proteins was expected as it is known to copurify with the TREX complex members (4–8). Notably, the ZC3H11A protein has been shown to interact with the THO core protein THOC2, TREX subunits POLDIP3 and UAP56(DDX39B) in an ATP-dependent and RNA-independent manner (7). The observations that the lack of ZC3H11A causes nuclear accumulation of polyadenylated mRNAs and that ZC3H11A interacts with the members of the TREX complex have put forward a model whereby the ZC3H11A protein regulates nuclear mRNA export (3, 7, 19). Surprisingly, the ZC3H11A protein also interacted with the PABPN1 protein, implying that it might be involved in mRNA 3′ end processing in addition to targeting the TREX complex and mRNA export. At least two studies have identified ZC3H11A as a PABPN1 interacting protein (46, 47). A previous study identified ZC3H11A as one of the PABPN1 interacting proteins under DNA damage response (DDR) conditions. However, the functional consequences of this interaction during DDR were not elucidated (46). Notably, we show that the PABPN1 protein interacts with the ZC3H11A ZFMs, which allowed us to dissect the functional consequences of the ZC3H11A-PABPN1 interaction (Fig. 3).

ZC3H11A is an RNA-binding protein, and the deletion of all three ZFMs abolished its binding to polyadenylated mRNAs (19). Further, based on the resemblance to other CCCH-type RNA-binding proteins (*e.g.*, ZAP or ZFP36) (3), it is predicted that the ZC3H11A ZFMs mediate its binding to mRNA. Therefore, it was surprising that PABPN1 interacted with the same protein region needed for the ZC3H11A RNA-binding activity. Our protein–protein interaction and protein–RNA binding experiments revealed that the mutation within the first ZFM (C8A) most efficiently blocked ZC3H11A interaction with PABPN1 and HAdV-5 mRNA (Figs. 3*C* and 8*A*). Although mutations within the other two ZFMs (C37A and C66A) also affected interaction with PABPN1 and viral mRNAs, the effects seen with the first ZFM (C8A) were the most drastic. Our experiments also suggest that ZC3H11A–PABPN1 interaction is partially mediated by poly(A)-containing RNA (Fig. 3*D*). Hence, it is possible that PABPN1 binding to poly(A) sequence may enhance ZC3H11A binding on the same mRNA molecule. Indeed, in PABPN1-depleted cells, the ZC3H11A protein binding to viral mRNAs was abolished (Fig. 8*B*). The PABPN1 depletion did not detectably affect the transfected ZC3H11A(wt)-Flag protein levels, indicating that reduced ZC3H11A RNA-binding was caused by the lack of the PABPN1 protein on targeted mRNAs. Since PABPN1 binds to the poly(A) tails, it implies that the ZC3H11A-RNA interactions should occur preferably at the 3′ end of mRNA. Indeed, a clear enrichment of the ZC3H11A protein binding at the 3′ end of both cellular and viral mRNAs has been shown (8, 19). Similarly, the preferential binding of the ZC3H11A protein at the 3′ end of cellular mRNAs was reported in a study analyzing the RNA-binding of 150 different RBPs (48). The same study also indicated that the ZC3H11A might be needed to export polyadenylated mRNAs. Together, our data and data from other studies suggest that the PABPN1 protein mediates ZC3H11A RNA-binding at the 3′ end of mRNA.

Since the PABPN1 protein controls the poly(A) tail synthesis and length (28), we also investigated if the ZC3H11A protein has an impact on poly(A) tail status using HAdV-5 as a model. Since reliable detection of the poly(A) tails is challenging, we used the PCR-based ePAT detection method, which can detect qualitative changes in the poly(A) tail (43). Indeed, our data show that the ePAT method is reliable as inhibition of pre-mRNA cleavage (siCPSF1-treatment) or poly(A) synthesis (siPABPN1-treatment) blocked detection of the oligoadenylated ((A_{12}), TVN-PAT) and polyadenylated (($A_{>12}$), ePAT) viral L3 and L5 mRNAs (Fig. 7, *B* and *C*). Interestingly, the absence of ZC3H11A did not detectably interfere with the oligoadenylation (A_{12}) of the L3 and L5 mRNAs but instead altered their polyadenylation ($A_{>12}$). More specifically, siZC3H11A treatment reduced L3 mRNA polyadenylation, whereas surprisingly, the length of the poly(A) tail was increased on the L5 mRNAs. These observations suggest that ZC3H11A acts specifically at the polyadenylation step (($A_{>12}$) and is probably fine-tuning the length of the poly(A) tail, depending on the mRNA origin (L3 *versus* L5). Since the ZC3H11A protein is not involved in PABPN1-dependent SNHG transcript turnover (Fig. 7*D*), we believe that the ZC3H11A-PABPN1 interaction is operational only in the canonical mRNA polyadenylation. This is also supported by the fact that ZC3H11A is not part of the PAXT complex, targeting polyadenylated SNHG transcripts for degradation (30). In our previous study, we showed that the lack of the ZC3H11A

protein caused nuclear retention of HAdV-5 mRNA in HeLa cells (19). It is reasonable to assume that one of the underlying reasons for that is altered polyadenylation of the viral transcripts, which will be retained in the cell nucleus. Hence, the data from our present and previous study (19) indicate that ZC3H11A might control HAdV-5 mRNA polyadenylation and the export of viral capsid mRNAs in HeLa cells.

Our study also reveals the details of the ZC3H11A protein subcellular localization. The ZC3H11A protein is known to localize into NS (19, 49), and based on our study, this localization pattern is controlled by the individual ZFMs (Fig. 4). All three tested ZFM mutations (C8A, C37A, C66A) blocked ZC3H11A co-localization with PABPN1 in NS. Further, after siPABPN1-treatment, ZC3H11A failed to associate with the NS (Fig. 5*A*). These observations indicate that PABPN1 is essential to keep ZC3H11A in the NS. This particular localization pattern raises a question of what is the function of the ZC3H11A-PABPN1 complex in the NS. The NS is proposed to regulate gene expression and RNA processing. This is supported by several MS studies showing that NS contains multiple splicing factors and proteins involved in mRNA polyadenylation (*e.g.*, CPSF1, PABPN1) (33, 50). Therefore, the ZC3H11A-PABPN1 interaction in the NS might either be needed to mark particular mRNA species for mRNA export or to control their poly(A) tail length.

Another important finding of our study was the identification of two NLSs in the ZC3H11A protein. Since the ZFM mutations or deletions did not expel the ZC3H11A protein from the nucleus, it was evident that the protein must contain strong NLS, which will drive its nuclear localization. Our two identified sequence elements fulfill the criteria for NLSs as both contain the basic amino acids (K and R). The N-terminal NLS, which was predicted to locate between aa 284 to 304, can be regarded as a bipartite NLS (BP-NLS) with the first three basic amino acids (K286, R287, and K288) separated from the last two basic amino acids (K300 and R301) by a 12 amino acid spacer sequence. Hence, the ZC3H11A BP-NLS resembles the BP-NLS previously identified in the 53BP1 and ING4 proteins (36). We did not do mutational analysis within the C-terminal NLS (aa 661–699), although the presence of the tripeptide motif KRK (aa 669–671) would suggest the presence of a monopartite NLS. Remarkably, only mutations of both NLS elements (KR5>A/Δ661–699) blocked ZC3H11A-KPNA3 interaction efficiently, which coincided with cytoplasmic localization of ZC3H11A (Fig. 6, *A* and *C*). However, our biochemical fractionation experiment revealed that the ZC3H11A(KR5>A/Δ661–699) still localized into the nucleus to some extent (Fig. 6*B*), indicating the possibility for an additional, uncharacterized NLS in the protein. Hence, our mutational analysis shows that two essential structural elements are needed for ZC3H11A to function as a nuclear protein. First, the integrity of the ZFMs is required for PABPN1-mediated ZC3H11A localization into the NS and binding to HAdV-5 capsid mRNAs. Second, the general localization of ZC3H11A into the cell nucleus is driven by the monopartite and bipartite NLSs and their interaction with the KPNA3 protein.

The ZC3H11A protein has a fast turnover rate in HeLa cells, although the mechanistic details about its proteasomal degradation have not been revealed (19). Notably, the cytoplasmic ZC3H11A (KR5>A/Δ661–699) was more stable compared to the wild-type protein (Fig. 6*D*), indicating that ZC3H11A might undergo proteasomal degradation in the nucleus. Indeed, a recent study has suggested that NS might act as the hotspot for the nuclear ubiquitination (51).

Collectively, our study reveals the human and mouse ZC3H11A interactomes and shows that the ZC3H11A protein specifically targets the PABPN1 protein and mRNA polyadenylation machinery.

Experimental procedures

Cell lines

A549 cells were obtained from ATCC. HEK293T and HeLa cells were obtained from Dr Johan Eriksson, Uppsala University, Sweden, and Dr Thomas Dobner, Leibniz Institute of Virology, Germany, respectively. The cell lines were grown in Dulbecco's modified Eagle medium (DMEM, Thermo Fisher Scientific) supplemented with 10% fetal bovine serum (FBS, Thermo Fisher Scientific) and penicillin-streptomycin solution (PEST, Thermo Fisher Scientific) at 37 °C in a 5% CO_2 incubator. The mESCs were obtained as a gift from Dr Alice Jouneau, Université Paris-Saclay, France. The mESCs were cultured on gelatin-coated plates and maintained in DMEM supplemented with 10% heat-inactivated FBS, penicillin (0.2 U/ml), streptomycin (0.2 μg/ml), L-glutamine (0.2 μg/ml) (Gibco) and with recombinant mouse Leukemia Inhibitory Factor (LIF, 20 U/ml, Millipore).

Generation of an A549-KO cell line

CRISPR/Cas9-edited A549 cells ($ZC3^{KO}$) were created as described previously (19). Briefly, a DNA fragment containing the U6 promoter, the gRNA sequence, the gRNA scaffold sequence, and a termination signal (IDT) was co-transfected to A549 cells with a Cas9-expressing plasmid and a linear hygromycin marker (Clontech). Transfected cells were cultured in selective media with 100 μg/ml of hygromycin B for 2 weeks. Control A549 cells (Cas9) were transfected only with the Cas9-expressing plasmid and a linear hygromycin marker. The resistant single-cell clones were isolated and screened for efficient ZC3H11A knockout by Western blotting.

Transfection, plasmids, and siRNA

All plasmid transfections were performed with JetPrime (Polyplus) transfection reagent according to the manufacturer's protocol. Plasmids expressing the PABPN1-Flag (NM_004643) and THOC5-HA (NM_001002878.1) proteins were purchased from GenScript. Plasmid pcDNA-THOC1-HA was generated by cloning the THOC1 sequence from plasmid phHpr1-GST (Addgene #11200) into pcDNA3(C-HA) background using BamHI/XhoI restriction enzymes. Plasmids expressing the ZC3H11A proteins were generated by cloning the ZC3H11A cDNA from pAcGFP1C1-ZC3H11A plasmid (19) into pcDNA3(C-HA) or pcDNA3(C-Flag) vectors using

EcoRI/XhoI restriction enzymes. The expressed ZC3H11A proteins contain C-terminal HA- or Flag-antibody epitope tags. Point mutations C8A, C37A, C66A, 3C>A (contains C8A, C37A, and C66A triple mutation), KR5>A (contains K286A, R287A, K288A, K300A, and R301A mutations) were done using QuikChange Mutagenesis Kit (Agilent). Deletion mutants (1–280, 1–530, 1–660, and 1–749) were generated using PCR primers annealing to the respective sequences. All three ZFM deletion mutant (ZC3H11A(dZF)) was generated by cloning the corresponding cDNA sequence (amino acids 87–810) from pAcGFP1C1-ZC3H11A($ZF^{\Delta 3}$) (19) into the pcDNA3(C-HA) and pcDNA3(C-Flag) plasmids. Mutation Δ661 to 699 was performed by cloning the ZC3H11A gBlock gene fragment (IDT) lacking the corresponding sequence into the pcDNA3-ZC3H11A(wt)-Flag vector using the PflMI and XhoI restriction enzymes. The siScr (5′-AGGUAGUGUAAUCGCCUUG-3′), siPABPN1 (5′-GUAGAGAAGCAGAUGAAUAdTdT-3′) and siCPSF1 (5′-GCAUUUCG CUGCUGCGCUA-3′) were purchased from Eurofins Genomics. siGENOME human ZC3H11A siRNA (M-021238-01-0005, Horizon Discovery) was used to knock down ZC3H11A mRNA. All siRNAs transfections (25 nM, 36–48 h) were done using JetPrime reagent.

Virus infection

Virus infections were done using replication-competent HAdV-5 as described previously (52). Replication-competent HAdV-5(NLuc) virus (generously provided by ZedCe Medicals AB, Sweden) was engineered by inserting the PGK-NLuc-poly(A) cassette from pNL1.1.PGK (Promega) plasmid into the virus genome. Infections were performed at a multiplicity of infection (MOI) of 5, defined as fluorescence-forming units (FFU/cell), in infection media (DMEM +2% FBS without any other supplements). After 1 h incubation at 37 °C in a 5% CO_2 incubator, virus-containing infection media was replaced with the normal growth media (DMEM containing FBS and PEST).

Co-immunoprecipitation, subcellular fractionation, and western blotting

HEK293T or HeLa cells were grown on six-well plates and transfected with the respective plasmids (2 μg of plasmid/well) for 36 h. Cells were harvested and lysed in 350 μl of lysis buffer (50 mM Tris-HCl pH7.5, 150 mM NaCl, 0.5% NP-40, 0.5% Triton X-100, 0.1% sodium deoxycholate, 0.2 μM $ZnCl_2$) supplemented with Halt protease inhibitors (Thermo Fisher Scientific) for 30 min on ice. The soluble cell lysate was immunoprecipitated with an anti-Flag(M2) affinity gel (A2220, Sigma) overnight at 4 °C. The beads were washed 2 × 1 ml in lysis buffer and 2 × 1 ml of lysis buffer containing 300 mM NaCl. Nuclease treatments were done by incubating soluble cell lysates in the presence of RNase A/T1 (Thermo Fisher Scientific, EN0551, final concentration 60 ng/μl of RNase A and 0.15 U/μl RNase T1), benzonase (Merck, E1014, final concentration 0.2 U/μl), or RNase I (Thermo Fisher Scientific, EN0601, final concentration 0.2 U/μl) on ice for 30 min. Thereafter the lysates were used for immunoprecipitation with an anti-Flag(M2) affinity gel overnight at 4 °C. Total RNA was isolated from nuclease-treated or non-treated cell lysates (ca. 20% of the whole lysate) using TRIzol LS reagent (Thermo Fisher Scientific) according to the manufacturer's protocol. Isolated RNA was separated on a 1% agarose gel (1× TBE) and visualized using GelRed dye (Biotium). Both inputs (corresponds to 5%) and immunoprecipitates were separated on 9% SDS-PAGE, transferred to a nitrocellulose membrane, and detected with the anti-Flag (rabbit, Sigma, F1804 or rabbit Proteintech, 20543-1-AP), anti-HA (mouse, Biolegend, MMS-101P) and anti-KPNA3 (rabbit, ABclonal, A8347) antibodies. Proteins were visualized with fluorescence-labeled secondary antibodies IRDye 680 or IRDye 800 (LI-COR) using the Odyssey CLX imaging system (LI-COR). Protein signals were quantified using either Fiji Image Processing (53) or Image Studio (LI-COR) software.

Subcellular fractionation of HeLa cells transfected with the ZC3H11A-Flag expressing plasmids (5 μg plasmid/100 mm tissue culture plate) was done using a Cell Fractionation Kit (Abcam, ab109719) according to the manufacturer's instructions. The anti-histone H3 (rabbit, Abcam, ab1791), anti-tubulin (mouse, Santa Cruz, sc-69969), and anti-Cox IV (rabbit, Proteintech, 11242-1-AP) antibodies were used to validate the purity of the nuclear, cytoplasmic and mitochondrial fractions, respectively. Whole-cell lysates were prepared as described previously (52), and proteins were detected using the anti-PABPN1 (rabbit, Abcam, ab75855), anti-ZC3H11A (rabbit, Abcam, ab99930), anti-CPSF1 (mouse, Santa Cruz, sc-166281), anti-GAPDH (mouse, Proteintech, 60004-1-Ig), anti-PABP (rabbit, Abcam, ab21060), and anti-actin (goat, Santa Cruz, c-1616) antibodies. Plasmid transfected HeLa cells were treated with cycloheximide (CHX, Sigma, C4859, 100 μg/ml as final concentration) 24 h post-transfection. Cells were collected 2, 4, and 8 h after the start of treatment, lysed, and analyzed by Western blotting as described previously (39).

Co-immunoprecipitation and MS sample preparation

HeLa cells were cultured in DMEM for Stable Isotope Labeling with Amino acids in Cell culture (SILAC, Thermo Fisher Scientific) supplemented with 10% dialyzed FBS (MWCO 10 kDa, Thermo Fisher Scientific), 100 U/ml of penicillin (Thermo Fisher Scientific), 100 μg/ml of streptomycin (Thermo Fisher Scientific), 0.25 μg/ml of amphotericin B (Thermo Fisher Scientific), and light isotopic labels L -arginine-HCl and L -lysine-2 HCl or heavy isotopic labels $^{13}C_6$, $_{15}$N4 l-arginine-HCl (Arg-10) and $^{13}C_6$, $^{15}N_2$ L-lysine-2 HCl (Lys-8) (Thermo Fisher Scientific). To avoid contamination of light amino acids, sub-culturing was performed using Cell dissociation buffer (Thermo Fisher Scientific) instead of trypsin. Isotopic incorporation was checked using a script in R as previously described (54) after approximately five cell divisions to assess complete (>95%) labeling. Conversion of arginine to proline was checked by calculating the percentage of heavy proline (Pro-6) containing peptides among all identified peptides and kept at <5%. Labeled HeLa cells (light or heavy) were grown on 100 mm tissue plates, and total protein

lysates were prepared using Pierce IP lysis buffer (Thermo Fisher Scientific) supplemented with protease inhibitors (Complete Ultra Tablets, Roche) and Pierce Universal Nuclease (Thermo Fisher Scientific). Lysates were cleared by centrifugation at 20,000*g* for 10 min at 4 °C and rotated end-over-end at 4 °C with anti-IgG (Abcam, light lysate) and anti-ZC3H11A (Atlas Antibodies, heavy lysate) antibodies in Protein LoBind tubes (Eppendorf). Thereafter, 30 µl of Dynabeads Protein G (Thermo Fisher Scientific) was added to each tube and incubated for 30 min at room temperature, followed by washing three times with Pierce IP lysis buffer. The bound proteins were eluted from the magnetic beads by adding 50 µl of elution buffer (5% SDS, 50 mM TEAB, pH 7.55) and heat-denatured for 5 min at 90 °C. Light (anti-IgG) and heavy (anti-ZC3H11A) eluted proteins were mixed 1:1.

HeLa cells were transfected with GFP-ZC3H11A(wt) or GFP-ZC3H11A(dZF) expressing plasmids. About 24 h post-transfection cells were lysed in 500 µl of Pierce IP lysis buffer (Thermo Fisher Scientific) supplemented with Halt protease inhibitors and benzonase nuclease (Merck, E1014, final concentration 0.25 U/µl). GFP-tagged proteins were immunopurified with GFP-Trap magnetic beads (Chromotek) for 1 h at 4 °C. Beads were washed four times in Pierce IP lysis buffer (containing Halt protease inhibitors). Proteins were eluted from the magnetic beads by adding 50 µl of elution buffer (5% SDS, 50 mM TEAB, pH 7.55) and heat denaturation for 5 min at 90 °C. Eluted proteins from either the SILAC co-IP or the GFP co-IP were treated by TCEP (5 mM) to reduce disulfide bonds, followed by adding methyl methanethiosulfonate to a final concentration of 15 mM to alkylate cysteines. After that, the lysate was acidified by adding phosphoric acid to a final concentration of 1.2%. The acidified lysate was added to an S-Trap microcolumn (Protifi) containing 300 µl of S-Trap buffer (90% MeOH, 100 mM TEAB, pH 7.5) and centrifuged at 4000*g* for 2 min. The S-Trap microcolumn was washed twice with S-Trap buffer. The columns were transferred to new tubes and incubated with 10 ng/µl sequencing-grade trypsin (Promega) (55). The digested proteins were eluted by centrifugation at 4000*g* for 1 min with 50 mM TEAB, 0.2% formic acid (FA), followed by 50% acetonitrile (ACN)/0.2% FA, and finally 80% ACN/0.1% FA. Peptides were dried in a vacuum centrifuge (Thermo Savant SPD SpeedVac, Thermo Fisher Scientific) and dissolved in 1% (v/v) FA.

Label-free co-IP of ZC3H11A-Flag was performed by transfecting HeLa cells on 100 mm tissue plates with pcDNA3 (control) or with pcDNA-ZC3H11A(wt)-Flag plasmids (Fig. S2). About 24 h post-transfection cells were lysed in 500 µl of Pierce IP lysis buffer supplemented with Halt protease inhibitors and benzonase nuclease (Merck, E1014, final concentration 0.25 U/µl). Flag-tagged ZC3H11A was immunopurified with anti-Flag(M2) magnetic beads (Sigma, M8823) overnight at 4 °C. Beads were washed four times in lysis buffer (lacking benzonase and protease inhibitors) and the proteins were eluted using 4× Laemmli sample buffer. Eluted proteins were loaded onto a 4 to 20% Mini-PROTEAN TGX precast gel (BioRad) and run approximately 2 cm in. The gel lanes were cut into two pieces (fractions), and proteins were reduced in-gel with 10 mM DTT in 25 mM NH_4HCO_3 (ABC), thereafter alkylated with 55 mM iodoacetamide in 25 mM ABC, and finally digested with 17 ng/µl sequencing-grade trypsin (Promega) in 25 mM ABC, using a slightly modified in-gel digestion protocol (55). Generated peptides were eluted from the gel pieces using 1% (v/v) FA in 60% (v/v) ACN, dried in a vacuum centrifuge (Thermo Savant SPD SpeedVac), and finally dissolved in 1% (v/v) FA. All peptides were desalted using Stage Tips (Thermo Fisher Scientific) and subsequently dissolved in 0.1% (v/v) FA in H_2O (solvent A) prior to LC-MS analyses.

Liquid chromatography and MS analysis

The desalted peptides were separated on an EASY-nLC 1000 UHPLC (Thermo Fisher Scientific) coupled to an Acclaim PepMap 100 column (2 cm × 75 µm, 3 µm particle size, Thermo Fisher Scientific) coupled in line with an EASY-Spray PepMap RSLC C18 reversed-phase column (50 cm × 75 µm, 2 µm particle size, Thermo Fisher Scientific). The column was heated to 35 °C and equilibrated with solvent A. A 2 to 40% gradient of solvent B (0.1% (v/v) FA in ACN) was run at 250 nl/min for 3 h. Eluted peptides were injected and analyzed on an Orbitrap Fusion Tribrid mass spectrometer (Thermo Fisher Scientific) controlled by the Xcalibur software (version 4.4.16.14, Thermo Fisher Scientific) and run at Top Speed data-dependent acquisition mode, a spray voltage of 2.4 kV, and an ion-transfer tube temperature of 275 °C. MS full scan spectra (m/z 400–2000) at a resolution of 120,000 at m/z 200 were collected in profile mode and analyzed in the Orbitrap with an automatic gain control target of 2.0e5, and a maximum injection time of 100 ms. Peptides with an intensity above 5.0e3 were selected for fragmentation utilizing collision-induced dissociation at a collision energy setting of 30%. Peptide fragments were analyzed in the linear ion trap with an automatic gain control of 1.0e4 and a maximum injection time of 40 ms, with the data acquired in centroid mode. A dynamic exclusion period of the peptides chosen for fragmentation was set to 60 s. The instrument setup quality control was monitored using the Promega 6 × 5 LC-MS/MS Peptide Reference Mix (Promega) and analyzed with the PReMiS software (version 1.0.5.1, Promega).

MS data analysis

Analysis of mass spectrometric raw files was performed using the MaxQuant quantitative proteomics software package (version 2.1.0.0), including the Andromeda search engine (56, 57). The search was conducted with cysteine methyl methanethiosulfonate (MMTS, SILAC co-IP, and GFP co-IP) or cysteine carbamidomethylation (label-free co-IP) as a static modification and methionine oxidation and protein N-terminal acetylation as variable modifications. MS1 Orbitrap tolerance was set to 20 ppm, and MS2 ion trap tolerance was set to 0.5 Da. Match between runs enabled identifying peptides where only MS1 data was available in one of the two fractions of each sample for the label-free co-IP, and re-quantify was set to on for the SILAC experiment, in case only one of the partners of a label pair was detected. Peaks were searched

against the UniProtKB/Swiss-Prot *Homo sapiens* proteome database (UP000005640, version 2022-04-28), and a maximum of two trypsin miscleavages per peptide was allowed. The MaxQuant potential contaminants database was also searched. A decoy search was made against the reversed database, with both peptide and protein false discovery rates set to 1%. Proteins identified with at least two peptides of at least seven amino acids in length were considered reliable.

The MaxQuant output was filtered by removing reversed database hits, proteins only identified by site, and potential contaminants. Proteins with more than one missing value in the three replicates were also filtered out. Normalization of LFQ intensity values was performed using the variance stabilization transformation (VSN) method (58), followed by imputation of missing values using the deterministic minimal value (MinDet) approach (59). The normalized intensities were fitted to a linear model. The significance of differentially enriched proteins was calculated using empirical Bayes moderated *t*-statistics, utilizing the DEP package for Bioconductor and R (version 1.6.0). *p*-values of the differentially enriched proteins were corrected for multiple testing using the Benjamini-Hochberg method.

Immunofluorescence assays

HeLa cells were seeded on coverslips and transfected with 0.25 μg of plasmid DNA. Cells were fixed in 4% paraformaldehyde for 10 min and permeabilized with 0.1% Triton X-100 in PBST (PBS + 0.01% Tween 20) for 10 min at room temperature. The cells on coverslips were blocked with blocking solution (2% BSA/PBST) for 30 min and incubated with the primary antibodies anti-Flag (mouse, Sigma, M2, F1804), anti-PABPN1 (rabbit, Abcam, ab75855), anti- SC35 (mouse, Abcam, ab11826) diluted in the blocking solution overnight at 4 °C. Proteins were visualized with the FITC- and TRITC-conjugated secondary antibodies (Sigma, F6005, and T5393) for 1 h at room temperature. Nuclei were stained with DAPI-supplemented Fluoromount-G mounting media (Thermo Fisher Scientific). Cells were visualized with a fluorescence microscope (Nikon eclipse 90i), and the images were analyzed with the NIS-elements (Nikon) software.

RNA crosslinking-immunoprecipitations followed by RT-qPCR

The CLIP-qPCR experiments were performed as described (60), with minor modifications. Shortly, transfected A549 cells were washed once with ice-cold 1× PBS and irradiated two times with 400 mJ/cm^2 (254 nm) in CL-1000 Ultraviolet Crosslinker (UVP). Quantitative reverse transcription PCR (qRT-PCR) reactions were performed using HOT FIREPOL EvaGreen Supermix (Solis BioDyne) in a QuantStudio 6 Flex Real-Time PCR System (Applied Biosystems). Every sample was analyzed in triplicate. Relative ZC3H11A binding to mRNA is shown after normalizing the immunoprecipitated reactions to the input. Primer sequences are available in Table S1.

Infectious virus determination

A549 cells were transfected with siScr, siZC3H11A, or siPABPN1 for 48 h, followed by HAdV-5(NLuc) virus infection (MOI = 1). Infected cells were collected at 24 h post-infection (hpi), lyzed in 100 μl of 0.1 M Tris-HCl (pH 8.0), freeze-thawed three times, and centrifuged to separate cell supernatant and cell debris. Equal volumes of the cell supernatant were used to re-infect fresh HeLa cells in a 96-well plate for 1 h. Cells were lysed 24 hpi in Passive Lysis Buffer (Promega), and NanoLuc luciferase reporter gene expression was detected using a Nano-Glo Luciferase Assay System (Promega) and analyzed on an Infinite M200 plate-reader (Tecan).

RNA isolation and qRT-PCR

Total RNA was isolated using TRIreagent (Sigma) and cleaned with the RapidOut DNA removal kit (Thermo Fisher Scientific). About 1 μg of RNA was used for cDNA synthesis using Maxima H minus reverse transcriptase (Thermo Fisher Scientific) and random primers. qRT-PCR reactions were performed as described above. Every sample was run in triplicate and normalized against the expression of the housekeeping gene HPRT1. Detailed viral and cellular primer sequences are available in Table S1.

TVN-PAT and ePAT experiments

HeLa cells were transfected with indicated siRNAs for 36 h, followed by HAdV-5 infection for an additional 24 h. Total RNA was isolated using TRIreagent (Sigma), DNaseI-treated (Thermo Fisher Scientific), and subjected to TVN-PAT and ePAT analysis essentially as described (43). Gene-specific and universal primers for TVN-PAT and ePAT reactions are described in Table S1. Semi-quantitative PCR amplifications were done using Phire Taq DNA polymerase (Thermo Fisher Scientific). PCR amplicons were separated on 2% Ultrapure agarose in 1× TAE buffer (Thermo Fisher Scientific) and were visualized with GelRed (Biotium).

Statistical analysis

Statistical analysis was performed in GraphPad Prism (9.4.0) statistical software (GraphPad). Results are expressed as mean, standard deviation (SD), or standard error of the mean (SEM). An unpaired *t* test was used to test for statistical significance (****$p \le 0.0001$; ***$p \le 0.001$; **$p \le 0.01$; *$p \le 0.05$; ns, not significant).

Data availability

The mass spectrometry proteomics data have been deposited to the ProteomeXchange Consortium (http://proteomecentral.proteomexchange.org) *via* the PRIDE partner repository (61) with the dataset identifier PXD042238.

Supporting information—This article contains supporting information.

Acknowledgments—We thank Dr Anette Carlsson for excellent technical support, Dr Wael Kamel, and the "ZC3H11A" group members for fruitful discussions.

Author contributions—L. A., T. P., and S. Y. conceptualization; K. K., E. S., Z. H., M. L., T. P., and S. Y. methodology; K. K., E. S., Z. H., M. L., P. D., T. P., and S. Y. validation; M. L., T. P., and S. Y. formal analysis; K. K., E. S., Z. H., M. L., P. D., M. D., T. P., and S. Y. investigation; L. A., G. A., T. P., and S. Y. resources; M. L. and S. Y. data curation; K. K., M. L., L. A., G. A., T. P., and S. Y. writing–original draft; M. L., M. D., L. A., G. A., T. P., and S. Y. writing–review and editing; K. K., E. S., Z. H., M. L., P. D., T. P., and S. Y. visualization; L. A., G. A., T. P., and S. Y. supervision; L. A., G. A., T. P., and S. Y. project administration; L. A. and G. A. funding acquisition.

Funding and additional information—The project was funded by the Knut and Alice Wallenberg Foundation (KAW 2017.0071).

Conflict of interest—The authors declare that they have no conflicts of interest with the contents of this article.

Abbreviations—The abbreviations used are: BP-NLS, bipartite NLS; CHX, cycloheximide; cNLS, classical NLS; CPSF1, cleavage and specificity factor 1; dZF, deletion of 3 ZFMs; ePAT, extension Poly(A) Test; FA, formic acid; FBS, fetal bovine serum; HAdV-5, human adenovirus type 5; mESCs, mouse embryonic stem cells; NLS, nuclear localization signal; NPC, nuclear pore complex; NS, Nuclear speckles; PABPN, poly(A) binding protein nuclear 1; PABPs, poly(A)-binding proteins; PAP, poly(A) polymerase; PAXT, poly(A) tail exosome targeting; RBPs, RNA-binding proteins; SNHG, snoRNA host gene; TREX, Transcription-Export; ZFM, zinc finger motifs.

References

1. Xie, Y., and Ren, Y. (2019) Mechanisms of nuclear mRNA export: a structural perspective. *Traffic* **20**, 829–840
2. Van Nostrand, E. L., Freese, P., Pratt, G. A., Wang, X., Wei, X., Xiao, R., *et al.* (2020) A large-scale binding and functional map of human RNA-binding proteins. *Nature* **583**, 711–719
3. Hajikhezri, Z., Darweesh, M., Akusjarvi, G., and Punga, T. (2020) Role of CCCH-type zinc finger proteins in human adenovirus infections. *Viruses* **12**, 1322
4. Dou, Y., Barbosa, I., Jiang, H., Iasillo, C., Molloy, K. R., Schulze, W. M., *et al.* (2020) NCBP3 positively impacts mRNA biogenesis. *Nucleic Acids Res.* **48**, 10413–10427
5. Dou, Y., Kalmykova, S., Pashkova, M., Oghbaie, M., Jiang, H., Molloy, K. R., *et al.* (2020) Affinity proteomic dissection of the human nuclear cap-binding complex interactome. *Nucleic Acids Res.* **48**, 10456–10469
6. Dufu, K., Livingstone, M. J., Seebacher, J., Gygi, S. P., Wilson, S. A., and Reed, R. (2010) ATP is required for interactions between UAP56 and two conserved mRNA export proteins, Aly and CIP29, to assemble the TREX complex. *Genes Dev.* **24**, 2043–2053
7. Folco, E. G., Lee, C. S., Dufu, K., Yamazaki, T., and Reed, R. (2012) The proteins PDIP3 and ZC11A associate with the human TREX complex in an ATP-dependent manner and function in mRNA export. *PLoS One* **7**, e43804
8. Younis, S., Jouneau, A., Larsson, M., Oudin, J. F., Adenot, P., Omar, J., *et al.* (2023) Ablation of ZC3H11A causes early embryonic lethality and dysregulation of metabolic processes. *Proc. Natl. Acad. Sci. U. S. A.* **120**, e2216799120
9. Heath, C. G., Viphakone, N., and Wilson, S. A. (2016) The role of TREX in gene expression and disease. *Biochem. J.* **473**, 2911–2935
10. Cheng, H., Dufu, K., Lee, C. S., Hsu, J. L., Dias, A., and Reed, R. (2006) Human mRNA export machinery recruited to the 5′ end of mRNA. *Cell* **127**, 1389–1400
11. Pacheco-Fiallos, B., Vorlander, M. K., Riabov-Bassat, D., Fin, L., O'Reilly, F. J., Ayala, F. I., *et al.* (2023) mRNA recognition and packaging by the human transcription-export complex. *Nature* **616**, 828–835
12. Katahira, J., Okuzaki, D., Inoue, H., Yoneda, Y., Maehara, K., and Ohkawa, Y. (2013) Human TREX component Thoc5 affects alternative polyadenylation site choice by recruiting mammalian cleavage factor I. *Nucleic Acids Res.* **41**, 7060–7072
13. Masuda, S., Das, R., Cheng, H., Hurt, E., Dorman, N., and Reed, R. (2005) Recruitment of the human TREX complex to mRNA during splicing. *Genes Dev.* **19**, 1512–1517
14. Morris, K. J., and Corbett, A. H. (2018) The polyadenosine RNA-binding protein ZC3H14 interacts with the THO complex and coordinately regulates the processing of neuronal transcripts. *Nucleic Acids Res.* **46**, 6561–6575
15. Lesbirel, S., Viphakone, N., Parker, M., Parker, J., Heath, C., Sudbery, I., *et al.* (2018) The m(6)A-methylase complex recruits TREX and regulates mRNA export. *Sci. Rep.* **8**, 13827
16. Fribourg, S., Braun, I. C., Izaurralde, E., and Conti, E. (2001) Structural basis for the recognition of a nucleoporin FG repeat by the NTF2-like domain of the TAP/p15 mRNA nuclear export factor. *Mol. Cell* **8**, 645–656
17. Viphakone, N., Hautbergue, G. M., Walsh, M., Chang, C. T., Holland, A., Folco, E. G., *et al.* (2012) TREX exposes the RNA-binding domain of Nxf1 to enable mRNA export. *Nat. Commun.* **3**, 1006
18. Yang, L., Wang, Z., Ouyang, H., Zhang, Y., Xiao, W., Liu, Y., *et al.* (2022) Porcine ZC3H11A is essential for the proliferation of pseudorabies virus and porcine circovirus 2. *ACS Infect. Dis.* **8**, 1179–1190
19. Younis, S., Kamel, W., Falkeborn, T., Wang, H., Yu, D., Daniels, R., *et al.* (2018) Multiple nuclear-replicating viruses require the stress-induced protein ZC3H11A for efficient growth. *Proc. Natl. Acad. Sci. U. S. A.* **115**, E3808–E3816
20. Droll, D., Minia, I., Fadda, A., Singh, A., Stewart, M., Queiroz, R., *et al.* (2013) Post-transcriptional regulation of the trypanosome heat shock response by a zinc finger protein. *PLoS Pathog.* **9**, e1003286
21. Darweesh, M., Younis, S., Hajikhezri, Z., Ali, A., Jin, C., Punga, T., *et al.* (2022) ZC3H11A loss of function enhances NF-kappaB signaling through defective IkappaBalpha protein expression. *Front. Immunol.* **13**, 1002823
22. Mangus, D. A., Evans, M. C., and Jacobson, A. (2003) Poly(A)-binding proteins: multifunctional scaffolds for the post-transcriptional control of gene expression. *Genome Biol.* **4**, 223
23. Zhao, L. W., and Fan, H. Y. (2021) Revisiting poly(A)-binding proteins: multifaceted regulators during gametogenesis and early embryogenesis. *Bioessays* **43**, e2000335
24. Kerwitz, Y., Kuhn, U., Lilie, H., Knoth, A., Scheuermann, T., Friedrich, H., *et al.* (2003) Stimulation of poly(A) polymerase through a direct interaction with the nuclear poly(A) binding protein allosterically regulated by RNA. *EMBO J.* **22**, 3705–3714
25. Kuhn, U., Gundel, M., Knoth, A., Kerwitz, Y., Rudel, S., and Wahle, E. (2009) Poly(A) tail length is controlled by the nuclear poly(A)-binding protein regulating the interaction between poly(A) polymerase and the cleavage and polyadenylation specificity factor. *J. Biol. Chem.* **284**, 22803–22814
26. Eckmann, C. R., Rammelt, C., and Wahle, E. (2011) Control of poly(A) tail length. *Wiley Interdiscip. Rev. RNA* **2**, 348–361
27. Banerjee, A., Apponi, L. H., Pavlath, G. K., and Corbett, A. H. (2013) PABPN1: molecular function and muscle disease. *FEBS J.* **280**, 4230–4250
28. Rodriguez-Molina, J. B., and Turtola, M. (2022) Birth of a poly(A) tail: mechanisms and control of mRNA polyadenylation. *FEBS Open Bio* **13**, 1140–1153
29. Beaulieu, Y. B., Kleinman, C. L., Landry-Voyer, A. M., Majewski, J., and Bachand, F. (2012) Polyadenylation-dependent control of long noncoding RNA expression by the poly(A)-binding protein nuclear 1. *PLoS Genet.* **8**, e1003078
30. Meola, N., Domanski, M., Karadoulama, E., Chen, Y., Gentil, C., Pultz, D., *et al.* (2016) Identification of a nuclear exosome decay pathway for processed transcripts. *Mol. Cell* **64**, 520–533

31. Bresson, S. M., Hunter, O. V., Hunter, A. C., and Conrad, N. K. (2015) Canonical Poly(A) polymerase activity promotes the decay of a wide variety of mammalian nuclear RNAs. *PLoS Genet.* **11**, e1005610
32. Apponi, L. H., Leung, S. W., Williams, K. R., Valentini, S. R., Corbett, A. H., and Pavlath, G. K. (2010) Loss of nuclear poly(A)-binding protein 1 causes defects in myogenesis and mRNA biogenesis. *Hum. Mol. Genet.* **19**, 1058–1065
33. Galganski, L., Urbanek, M. O., and Krzyzosiak, W. J. (2017) Nuclear speckles: molecular organization, biological function and role in disease. *Nucleic Acids Res.* **45**, 10350–10368
34. Lin, Y., Robbins, J. B., Nyannor, E. K., Chen, Y. H., and Cann, I. K. (2005) A CCCH zinc finger conserved in a replication protein a homolog found in diverse Euryarchaeotes. *J. Bacteriol.* **187**, 7881–7889
35. Spector, D. L., and Lamond, A. I. (2011) Nuclear speckles. *Cold Spring Harb. Perspect. Biol.* **3**, a000646
36. Lu, J., Wu, T., Zhang, B., Liu, S., Song, W., Qiao, J., *et al.* (2021) Types of nuclear localization signals and mechanisms of protein import into the nucleus. *Cell Commun. Signal.* **19**, 60
37. Kosugi, S., Hasebe, M., Tomita, M., and Yanagawa, H. (2009) Systematic identification of cell cycle-dependent yeast nucleocytoplasmic shuttling proteins by prediction of composite motifs. *Proc. Natl. Acad. Sci. U. S. A.* **106**, 10171–10176
38. Miyamoto, Y., Yamada, K., and Yoneda, Y. (2016) Importin alpha: a key molecule in nuclear transport and non-transport functions. *J. Biochem.* **160**, 69–75
39. Inturi, R., Thaduri, S., and Punga, T. (2013) Adenovirus precursor pVII protein stability is regulated by its propeptide sequence. *PLoS One* **8**, e80617
40. Tudek, A., Lloret-Llinares, M., and Jensen, T. H. (2018) The multitasking polyA tail: nuclear RNA maturation, degradation and export. *Philos. Trans. R. Soc. Lond. B Biol. Sci.* **373**, 20180169
41. Donovan-Banfield, I., Turnell, A. S., Hiscox, J. A., Leppard, K. N., and Matthews, D. A. (2020) Deep splicing plasticity of the human adenovirus type 5 transcriptome drives virus evolution. *Commun. Biol* **3**, 124
42. Westergren Jakobsson, A., Segerman, B., Wallerman, O., Lind, S. B., Zhao, H., Rubin, C. J., *et al.* (2020) The human adenovirus type 2 transcriptome: an amazing complexity of alternatively spliced mRNAs. *J. Virol.* **95**, e01869–e01920
43. Janicke, A., Vancuylenberg, J., Boag, P. R., Traven, A., and Beilharz, T. H. (2012) ePAT: a simple method to tag adenylated RNA to Measure poly(A)-tail length and other 3' RACE applications. *RNA* **18**, 1289–1295
44. Clerici, M., Faini, M., Aebersold, R., and Jinek, M. (2017) Structural insights into the assembly and polyA signal recognition mechanism of the human CPSF complex. *Elife* **6**, e33111
45. Tsoukas, R. L., Volkwein, W., Gao, J., Schiwon, M., Bahlmann, N., Dittmar, T., *et al.* (2022) A human in vitro model to study adenoviral receptors and virus cell interactions. *Cells* **11**, 841
46. Gavish-Izakson, M., Velpula, B. B., Elkon, R., Prados-Carvajal, R., Barnabas, G. D., Ugalde, A. P., *et al.* (2018) Nuclear poly(A)-binding protein 1 is an ATM target and essential for DNA double-strand break repair. *Nucleic Acids Res.* **46**, 730–747
47. Kwiatek, L., Landry-Voyer, A. M., Latour, M., Yague-Sanz, C., and Bachand, F. (2023) PABPN1 prevents the nuclear export of an unspliced RNA with a constitutive transport element and controls human gene expression via intron retention. *RNA* **29**, 644–662
48. Van Nostrand, E. L., Pratt, G. A., Yee, B. A., Wheeler, E. C., Blue, S. M., Mueller, J., *et al.* (2020) Principles of RNA processing from analysis of enhanced CLIP maps for 150 RNA binding proteins. *Genome Biol.* **21**, 90
49. Ilik, I. A., Malszycki, M., Lubke, A. K., Schade, C., Meierhofer, D., and Aktas, T. (2020) SON and SRRM2 are essential for nuclear speckle formation. *Elife* **9**, e60579
50. Faber, G. P., Nadav-Eliyahu, S., and Shav-Tal, Y. (2022) Nuclear speckles - a driving force in gene expression. *J. Cell Sci.* **135**, jcs259594
51. Marzahn, M. R., Marada, S., Lee, J., Nourse, A., Kenrick, S., Zhao, H., *et al.* (2016) Higher-order oligomerization promotes localization of SPOP to liquid nuclear speckles. *EMBO J.* **35**, 1254–1275
52. Mun, K., and Punga, T. (2019) Cellular Zinc Finger Protein 622 Hinders Human Adenovirus Lytic Growth and Limits Binding of the Viral pVII Protein to Virus DNA. *J. Virol.* **93**, e01628–e01718
53. Schindelin, J., Arganda-Carreras, I., Frise, E., Kaynig, V., Longair, M., Pietzsch, T., *et al.* (2012) Fiji: an open-source platform for biological-image analysis. *Nat. Methods* **9**, 676–682
54. Stöhr, G., and Tebbe, A. (2011) Chapter 8. Quantitative LC-MS of proteins. In: Letzel, T., ed. *Protein and Peptide Analysis by LC-MS: Experimental Strategies*, The Royal Society of Chemistry, Cambridge, UK: 104–122
55. Shevchenko, A., Wilm, M., Vorm, O., and Mann, M. (1996) Mass spectrometric sequencing of proteins silver-stained polyacrylamide gels. *Anal. Chem.* **68**, 850–858
56. Cox, J., Matic, I., Hilger, M., Nagaraj, N., Selbach, M., Olsen, J. V., *et al.* (2009) A practical guide to the MaxQuant computational platform for SILAC-based quantitative proteomics. *Nat. Protoc.* **4**, 698–705
57. Tyanova, S., Temu, T., and Cox, J. (2016) The MaxQuant computational platform for mass spectrometry-based shotgun proteomics. *Nat. Protoc.* **11**, 2301–2319
58. Huber, W., von Heydebreck, A., Sultmann, H., Poustka, A., and Vingron, M. (2002) Variance stabilization applied to microarray data calibration and to the quantification of differential expression. *Bioinformatics* **18**, S96–S104
59. Lazar, C., Gatto, L., Ferro, M., Bruley, C., and Burger, T. (2016) Accounting for the multiple natures of missing values in label-free quantitative proteomics data sets to compare imputation strategies. *J. Proteome Res.* **15**, 1116–1125
60. Hajikhezri, Z., Kaira, Y., Schubert, E., Darweesh, M., Svensson, C., Akusjarvi, G., *et al.* (2023) Fragile X-Related Protein FXR1 Controls Human Adenovirus Capsid mRNA Metabolism. *J. Virol.* **97**, e0153922
61. Perez-Riverol, Y., Csordas, A., Bai, J., Bernal-Llinares, M., Hewapathirana, S., Kundu, D. J., *et al.* (2019) The PRIDE database and related tools and resources in 2019: improving support for quantification data. *Nucleic Acids Res.* **47**, D442–D450